Nationaal Lucht- en Ruimtevaartlaboratorium
National Aerospace Laboratory NLR

NLR-TP-2000-358

Microstructural embrittlement of gold and silver

R.J.H. Wanhill

This report has been prepared as a contribution to the archaeometallurgical literature.

Division: Structures and Materials
Issued: 4 July 2000
Classification of title: Unclassified

Contents

(66 pages in total)

MICROSTRUCTURAL EMBRITTLEMENT OF GOLD AND SILVER

R.J.H. Wanhill
National Aerospace Laboratory NLR, Anthony Fokkerweg 2,
1059 CM Amsterdam, The Netherlands

ABSTRACT

Empirical and theoretical metallurgical knowledge enables specifying which elements, in amounts less than about 5 at. %, could embrittle or impair the mechanical properties of gold and silver. There are two categories of this microstructurally-induced embrittlement: alloys most probably embrittled as-cast, and alloys that could be embrittled by low temperature ageing. From the chemical compositions and current evidence for microstructural embrittlement of *archaeological* gold and silver, the most likely embrittling elements are lead, bismuth and antimony, especially lead. As yet there is no good evidence for microstructural embrittlement of archaeological gold. But archaeological silver can suffer age-embrittlement, most probably due to lead. Suggestions for further investigation are made.

KEYWORDS: ARCHAEOLOGICAL GOLD AND SILVER, EMBRITTLEMENT, CRACKS AND FRACTURE, IMPURITY AND ALLOYING ELEMENTS, PHASE DIAGRAMS, MICROSTRUCTURE, PRECIPITATION, SEGREGATION.

INTRODUCTION

Gold and silver are normally soft, ductile and easily fabricated. However, both can be embrittled by small amounts of metallic impurities or alloying elements. The purpose of this report is to discuss and explain this microstructurally-induced embrittlement and examine its significance for archaeological gold and silver.

EVIDENCE OF EMBRITTLEMENT

Gold

The first systematic evidence of gold embrittlement was obtained by Hatchett (1803). He added small quantities of metals to fine gold (99.5 wt. % Au) or standard coinage gold (Au-8 wt. % Cu) and showed, by hammering or bending, that some of the as-cast alloys were brittle. The

most detrimental additions were arsenic, antimony, lead and bismuth. Arsenic embrittled fine gold down to 0.1 wt. %, and antimony, lead and bismuth embrittled standard gold down to about 0.05 wt. %.

Following Hatchett's work, Roberts-Austen (1888) prepared and mechanically tested cast bars of binary gold alloys. These contained about 0.2 wt. % of elements selected from all the Groups in the Periodic Table. Roberts-Austen plotted the mechanical properties against the theoretical atomic volumes of the alloying elements. Analogous plots are given in figure 1, which, however, uses the atomic diameters of the elements when alloyed with gold, see footnote (2) in table 1.

Figure 1 shows that elements with larger alloying atomic diameters tend to be more detrimental to the mechanical properties, in particular potassium, lead, bismuth and tellurium. Roberts-Austen reported that the fracture surfaces of bars containing these elements, as well as bars containing antimony, indium or thallium, had a marked "crystalline structure". In modern parlance this means fracture occurred partly or wholly along the crystal or grain boundaries that formed during solidification of the cast bars. Grain boundary fracture is a sign of weakness or embrittlement in normally ductile metals (Thompson and Knott 1993) and is often the result of impurity element segregation to the grain boundaries (Shewmon 1998).

Silver

It has long been known that certain elements can embrittle silver, notably lead and tin (Ercker 1574) and antimony (Gowland 1918). The first detailed investigation appears to be due to Thompson and Chatterjee (1954). They studied the embrittlement of silver by age-hardening (age-embrittlement), prompted by the brittleness of archaeological silver coins that must have been ductile when struck.

Thompson and Chatterjee analysed fifteen brittle silver coins, finding copper and lead in appreciable quantities, but no other element except as a trace. The copper contents were up to several weight % and the lead contents varied from 0.25-1.6 wt. %. From these analyses they considered that embrittlement could be due to age-hardening owing to precipitation of lead from supersaturated solid solution in the silver matrix of Ag-Pb or Ag-Cu-Pb alloys. They provided evidence for this possibility as follows:

(1) By determining the silver-rich low temperature region of the Ag-Pb phase diagram, figure 2. This required weeks and months of ageing supersaturated solid solutions of lead

in silver, and showed that a lead-rich phase (β) precipitates out of solution even at very low lead contents, less than 0.1 wt. %, and down to ambient temperatures.

(2) By mechanically testing age-hardened Ag-Pb and Ag-Cu-Pb alloys, figure 3, and showing that prolonged ageing led to brittle fracture.

However, lead-rich precipitates may not be necessary. Wanhill *et al.* (1998) examined a severely embrittled Egyptian silver vase, figure 4a. Microstructural embrittlement was characterized by "clean" grain boundary fracture with no sign of precipitates. This is illustrated in figure 4b, with the caveat that features on the grain boundary facets are due to localised corrosion after fracture. In view of the vase metal analysis (in weight %: 97.1 Ag-0.9 Cu-0.8 Au-0.7 Pb-0.3 Sb-0.2 Sn) and a theory of adsorption-induced embrittlement (Seah 1980a), Wanhill *et al.* concluded that embrittlement could have been due to lead atoms segregating to grain boundaries and reducing their cohesive strength (Wanhill *et al.* 1998; Wanhill 1998).

Be that as it may, Thompson and Chatterjee (1954) made the essential point that the type of embrittlement they studied was age-embrittlement, whereby the silver alloys were initially ductile, but the type of embrittlement investigated by Roberts-Austen (1888) was present directly in as-cast gold alloy bars.

EMPIRICAL AND THEORETICAL METALLURGICAL CONSIDERATIONS

The starting point for this section is the observation that gold is embrittled by elements having very low solid solubilities in it (Shewmon 1998). The topics are: primary solid solubility; equilibrium grain boundary segregation; and alloy phase diagrams, non-equilibrium cooling and mechanical behaviour.

Primary solid solubility

Primary solid solubility is governed by atomic size differences between the solute and solvent and by the tendency to form intermediate phases and intermetallic compounds. These observations can be expressed, in order of importance, by the size-factor rule, the electrochemical differences and hence chemical affinities of the alloying components, and the electron concentration change upon alloying (Hume-Rothery and Raynor 1954; Pettifor 1984, 1988; Massalski 1996).

The size-factor rule states that when the atomic diameters of solute and solvent differ by more than 14-15 %, the size-factor is unfavourable and the primary solid solubility will generally be restricted to a few atomic per cent. It is, however, a negative rule: favourable size-factors do not

necessarily mean high solid solubilities. Figure 5 illustrates the rule for solid solutions in gold and silver. Rubidium, potassium and sodium have very unfavourable size-factors and, as table 1 shows, zero solid solubility. They are followed by lead, bismuth and thallium, with solid solubilities less than 8 at. %.

In the case of gold we can compare figure 5 with figure 1. Of the four most embrittling elements investigated by Roberts-Austen (1888), potassium, lead and bismuth have unfavourable size-factors and zero or very low solid solubilities. Tellurium is the exception in terms of size-factor, and this leads to the next criterion, electrochemical difference and chemical affinity.

The greater the electrochemical difference between solute and solvent, the greater is their affinity and tendency to form intermediate phases and intermetallic compounds. In turn, this means primary solid solubility will be restricted (Hume-Rothery and Raynor 1954; Massalski 1996). The electrochemical difference is quantifiable by differences in electronegativity of the alloying components (Pauling 1945, 1947; Darken and Gurry 1953; Gordy and Thomas 1956).

Much effort has been put into combining the size-factor rule and electronegativity differences on Darken-Gurry (D-G) maps, e.g. Darken and Gurry (1953), Waber *et al.* (1963), Gschneider (1980). D-G maps are supposed to enable predictions whether solid solubility is low or moderate-to-high. Figure 6 shows D-G maps for solid solutions in gold and silver, using data from table 1. Solute elements outside each solvent's ellipse should have low solid solubilities, while elements within the ellipse are predicted to have solid solubilities greater than 5-10 at. %. However, again using table 1, we see that for gold this latter prediction is incorrect with respect to rhodium, germanium, arsenic, antimony and tellurium, and for silver with respect to tellurium. Also, lithium is incorrectly predicted to have low solid solubility in gold and silver, as are palladium, arsenic and antimony in silver.

These and other inadequacies of D-G maps have been explained by Gschneider (1980) in a general way, i.e. not specifically considering gold and silver as the solvents. To overcome these inadequacies Gschneider presented several new rules, which he realised would make D-G maps largely unnecessary.

More recently, Pettifor (1984, 1988) derived a series of the elements that goes beyond electronegativity by also acknowledging the chemical similarity of elements from the same Group of the Periodic Table. Each element is given an empirical ordering number, and examples are given in table 1. Pettifor demonstrated the usefulness of this deceptively simple empirical approach by showing it enabled systematic separation of the crystal structures of many binary intermetallic compounds.

The third factor to consider is the electron concentration, which is the ratio of valence electrons to the number of atoms. Empirical studies of binary gold, silver and copper alloys, in particular with B-subGroup elements, have shown that when the effects of size-factor and electrochemical difference are "relatively small", the primary solid solubility limits occur at fairly constant values of electron concentration (Hume-Rothery and Raynor 1954). In a famous theory, Jones (1937) provided an explanation of this phenomenon and derived a theoretical critical electron concentration of 1.41.

Figure 7 illustrates the electron concentration effect for binary gold and silver alloys, whereby the solutes have favourable size-factors but the combination of electronegativity and chemical differences, expressed by Pettifor's empirical ordering sequence, increases in going from cadmium to antimony. Most of the alloys have primary solid solubility limits at electron concentrations between 1.21-1.33 (gold) and 1.35-1.42 (silver). The latter agree with Jones' theoretical value of 1.41, but the lower values for gold alloys are anomalous. Hume-Rothery and Raynor (1954) suggested this anomaly could be due to gold's general tendency to be more highly ionised than silver, such that gold ions in the alloys contribute more than one valence electron. This means that the critical electron concentration, and hence the primary solid solubility limit, would be reached at lower solute contents. Whether or not this suggestion is correct, and although there are problems with Jones' theory (Cottrell 1988; Massalski 1996), the fact remains that many of the elements listed in table 1 have lower primary solid solubilities in gold than in silver.

Equilibrium grain boundary segregation

Equilibrium grain boundary segregation involves the solid state redistribution of solute elements and their adsorption at grain boundaries. Solutes of low solubility generally segregate strongly and vice versa (Seah 1980b). Another important characteristic is that at the commonly observed levels of segregation many elements co-segregate rather than compete for grain boundary adsorption sites (Hondros and Seah 1977; Seah 1980b).

This type of segregation can greatly reduce the cohesive strength of grain boundaries, leading to grain boundary fracture and embrittlement (Seah 1980a, 1980b; Shewmon 1998), and Seah (1980a) has developed a theory of embrittlement owing to adsorption-induced grain boundary decohesion. Figure 8 shows the theory's predictions for segregant elements in gold and silver. This figure should be interpreted as follows: elements with sublimation enthalpies lower than those of the matrix will, *if segregated*, cause embrittlement of the matrix grain boundaries, and the embrittling effect will be greater the lower the sublimation enthalpy of the segregant

element. (The sublimation enthalpy is a measure of the heat required to evaporate atoms from the solid surface of an element.)

Figure 9 correlates alloying element primary solid solubility limits in gold and silver with their sublimation enthalpies. The elements are arranged according to Pettifor's (1988) empirical ordering numbers, unfavourable size-factors are indicated, and it is also seen that most elements from cadmium onwards have lower solid solubilities in gold. The shaded regions in figure 9 indicate the matrix and alloying element combinations that would seem most likely to result in segregation-induced grain boundary fracture under equilibrium conditions: gold and silver containing sodium, potassium, rubidium, lead, bismuth, tellurium and selenium, and gold containing thallium, germanium, antimony and arsenic. There are other possibilities also, notably gold containing tin, and silver containing thallium, tin, antimony and arsenic.

However, the key question, unanswerable by figures 8 and 9, is whether the indicated alloying elements actually segregate to grain boundaries to cause embrittlement. Another important question is whether they might cause embrittlement in another way. To try to answer these questions, and also to explain the observed embrittlement of gold and silver discussed earlier, it is necessary to consider the alloy phase diagrams, the effects of non-equilibrium cooling on the phase changes, and the likely mechanical behaviour of the alloys.

Alloy phase diagrams, non-equilibrium cooling, and mechanical behaviour

Table 2 lists the equilibrium phase diagram characteristics and ambient temperature phases for dilute gold and silver binary alloys whose alloying elements have low primary solid solubilities.

Phase changes for the alloys in sub-table 2.1 should be independent of cooling rate, within normal metallurgical variations, except for the possible low temperature solid state decomposition of Au_2Bi, likely to be suppressed by fast cooling. This basic independence of cooling rate means that in the as-cast condition there will always be intercrystalline or intergranular phases. Many are intermetallic compounds, which are usually brittle and cause poor mechanical behaviour. Roberts-Austen's (1888) data, figure 1, provide evidence for this, specifically for gold alloyed with potassium, lead, bismuth and tellurium.

Phase changes for the alloys in sub-tables 2.2 and 2.3 will depend on cooling rate. This will be illustrated with the aid of figure 10, which shows schematic binary alloy equilibrium phase diagrams involving eutectic or peritectic reactions. Consider two dilute alloys whose bulk compositions approach the primary solid solubility limits, α_3, and are represented by the

vertical lines meeting the abscissae at X. Non-equilibrium cooling has two major effects on the phase changes:

(1) If cooling is fast enough the solidification compositions follow the curves α_1–α_3' rather than α_1–α_3. This means the solid solubilities are reduced, final solidification is at temperatures T_3 instead of T_2, the last liquids to solidify have compositions L_3 instead of L_2, and the alloys do not finally solidify only as α. Instead the eutectic or peritectic reactions occur at T_3: the remaining liquids either solidify as eutectic $\alpha+\beta$ between the primary α crystals or grains, or else react – the peritectic reaction – with some of the primary α crystals or grains to form β between them.

(2) Suppression of solid state reactions (already mentioned concerning Au-Bi alloys) and the retention of metastable phases down to ambient temperatures. This is possible because the diffusion of atoms is much slower in solids than in liquids. From figure 10 we see that under equilibrium conditions the two alloys undergo solid state partial decomposition ($\alpha \rightarrow \alpha+\beta$) at temperatures below T_4. However, faster cooling will cause supersaturated α to be retained, at least temporarily, down to ambient temperatures.

These effects may be interpreted to some extent for the alloys in sub-tables 2.2 and 2.3. Firstly, non-equilibrium cooling could cause alloys with bulk compositions below $PSSL_{max}$ or $PSSL_{eut}$ to finally solidify as though their bulk compositions were above these limits, leading to poor mechanical properties. *Indirect* evidence for this is the behaviour of gold containing thallium. In this system the solid solubility of thallium becomes zero well above the eutectic temperature, resulting in eutectic Au+Tl between the primary crystals or grains however dilute the alloy. Roberts-Austen (1888) noted the "crystalline structure" of the fracture surface of an as-cast Au-0.2 wt. % ($\approx$ 0.2 at. %) Tl bar, and figure 1 shows its tensile elongation was low.

Secondly, the solid state decomposition reactions listed in the last two columns of sub-tables 2.2 and 2.3 could be partially or wholly prevented by non-equilibrium cooling. Subsequent ageing at low or even ambient temperatures could then result, in some cases, in alloying element segregation and precipitation, and mechanical behaviour deterioration and embrittlement. The archetype is provided by the Ag-Pb alloy experiments of Thompson and Chatterjee (1954), discussed in the previous section of this report and illustrated by figures 2 and 3.

Other systems that are candidates for mechanical behaviour deterioration and embrittlement owing to alloying element solid state segregation are gold containing germanium, tin (Hondros *et al.* 1996) and antimony; and silver containing arsenic, bismuth and thallium. The Ag-Sb and Ag-Sn systems are less likely to belong to this category, even though antimony and tin can

embrittle silver (Ercker 1574; Gowland 1918). This is because the solid solubilities of antimony and tin in silver are still significant at ambient temperatures, sub-table 2.2. Also, the Ag-Ge system would appear to be excluded, since germanium has a higher sublimation enthalpy than silver, table 1 and figures 8 and 9.

Summary

Empirical and theoretical metallurgical knowledge enables specifying which elements, in amounts less than about 5 at. %, could embrittle or impair the mechanical behaviour of gold and silver. There are two categories, alloys most probably embrittled as-cast, and alloys that could be embrittled by low temperature ageing. These categories are given below, whereby asterisks indicate known embrittlement or poor mechanical behaviour of dilute alloys (Hatchett 1803; Roberts-Austen 1888; Thompson and Chatterjee 1954; Raub 1995).

(1) As-cast : Au-As*, Au-Bi*, Au-Ge, Au-K*, Au-Na, Au-Pb*, Au-Rb, Au-Sb*, Au-Se, Au-Te*, Au-Tl*; Ag-Bi, Ag-K, Ag-Na, Ag-Pb, Ag-Rb, Ag-Se, Ag-Te*.
(2) Aged : Au-Ge, Au-Sb, Au-Sn; Ag-As, Ag-Bi, Ag-Pb*, Ag-Tl.

For both categories the presence of more than one of the specified elements in gold or silver could be cumulatively detrimental. This seems likely for aged alloys since, as remarked earlier, many elements co-segregate rather than compete for grain boundary adsorption sites.

COMPOSITIONS OF ARCHAEOLOGICAL GOLD AND SILVER

Gold

Both native and pyrometallurgically processed gold alloys have been used for archaeological artifacts, e.g. Tylecote (1987). Chemical analyses have often been limited to the main alloying elements gold, silver and copper, but extensive compilations including more detailed analyses exist (Hartmann 1970, 1982; Taylor 1980; Eluère 1982). In particular, Hartmann analysed for several minor or trace elements, including the known embrittling elements arsenic, antimony, lead and bismuth. From these and other data some distinctions can be made between native and processed gold:

(1) *Main elements*. The silver content of native and processed gold varies widely, from less than 1 wt. % to 40 wt. % (native gold) or more: see for example Hartmann (1970, 1982), Tylecote (1986, 1987), Hauptmann *et al.* (1995) and Pingel (1995).

The copper content of native gold is limited, usually no more than 2 wt. % (Pingel 1995). But copper in processed gold often reaches 5-10 wt. % and exceptionally can be more than 50 wt. % (Pingel 1995; Waldhauser 1995). Note, however, that gold coins historically have been severely debased, with copper sometimes exceeding 70 wt. % (Oddy and La Niece 1986).

(2) *Other elements.* Native gold usually has only traces, less than 0.1 wt. %, of other elements. Mercury is most often reported, less frequently iron, tin and lead, and more rarely platinum, zinc, bismuth, arsenic, antimony and tellurium (Tylecote 1986, 1987; Raub 1995; Hauptmann *et al.* 1995).

Processed gold differs, depending partly on the overall purity. Table 3 classifies several impurity elements in native and processed gold lying within two ranges of high gold content. Unlike native gold, processed gold often contains tin but not mercury, and its tin content tends to increase with decreasing overall purity. Also, though there are few detailed analyses of native gold, it does appear that platinum is more likely to occur in processed gold, and lead too, in the lower purity range. There is additional evidence for these "trends". Platinum Group Element (PGE) inclusions occur rather frequently in gold jewellery and coins (Ogden 1977; Meeks and Tite 1980). And Hartmann's compilations show that higher silver contents and especially higher copper contents, well above the 2 wt. % limit of native gold, increase the occurrence of trace or minor amounts of antimony, lead and bismuth.

Silver

Native silver alloys may or may not have been used for Old World archaeological artifacts (Lucas 1928; Gale and Stos-Gale 1981a; Philip and Rehren 1996). However, the general scarcity of native silver compared to silver-containing minerals, mostly lead ores, and the early development of lead cupellation resulted in pyrometallurgy becoming the main source of silver (Gowland 1918; Gale and Stos-Gale 1981a, 1981b; Tylecote 1986; Raub 1995).

Cupellation is very effective in producing silver above 95 wt. % purity (Tylecote 1986, 1987), though it usually contains minor-to-trace amounts of gold, copper, lead and bismuth, and traces of antimony, arsenic, tellurium, zinc and nickel (McKerrell and Stevenson 1972; Gale and Stos-Gale 1981a; Raub 1995). Gold, copper, lead and bismuth contents are generally below 1 wt. % for each element: higher copper and lead contents in finished artifacts and coins, and also tin or zinc above 0.1 wt. %, suggest or indicate deliberate alloying, see McKerrell and Stevenson (1972) and Gale and Stos-Gale (1981a).

Figure 11 quantifies actually or potentially embrittling elements found in archaeological silver artifacts and coins lying within two ranges of high silver content. Though there are wide variations, lead is the main impurity, averaging 0.5-1 wt. %. Bismuth, antimony and tin are generally below 0.5 wt. %.

DISCUSSION

Archaeological gold embrittlement

Macroscopic photographs and drawings of damaged archaeological gold artifacts in Hartmann (1970, 1982) were assessed by the author for evidence of brittle fracture, see Appendix C. One artifact, sample number 575 and shown in figure C.2, was assessed to have *probably* undergone brittle fracture, forty-one as containing *possibly* brittle I fractures, and ninety-six as containing *possibly* brittle II fractures, in decreasing order of likelihood.

Figure 12 shows the assessment results in a silver-copper compositional diagram, which includes two important boundaries for Au-Ag-Cu alloys: the primary solid solubility limit and the lower limit of susceptibility to stress corrosion cracking. These boundaries are derived from modern alloy research, which means they are useful but perhaps not definitive for ancient gold alloys.

With this caveat in mind, the artifact data in figure 12 indicate that most of the more or less brittle-looking damage is unlikely to be attributable to a loss of ductility owing to long-term formation of Au-Cu ordered phases in the alloys (Prince *et al.* 1990) or to stress corrosion cracking. Conversely, two or three of the artifacts in Hartmann (1982), sample numbers 3619, 3829 and 4447, have crack patterns *suggesting* stress corrosion cracking. The clearest example, sample number 3619, is in figure C.4 of the present report.

The other potential causes of brittle-looking damage are ductile tearing of thin materials, corrosion and microstructural embrittlement:

(1) *Ductile tearing.* In thin materials ductile tearing can give a macroscopic impression of low ductility or even brittleness. Since nearly all the artifacts in Hartmann (1970, 1982) were made of thin materials, it is possible or probable that ductile tearing was responsible for much or most of the observed damage.

(2) *Corrosion.* Crack-like damage by corrosion is unlikely, for two reasons. First, most artifacts exceeded 18k purity, see figure 12, which implies high corrosion resistance.

Second, corrosion in high-karat gold alloys results in thin porous outer layers (Lehrberger and Raub 1995; Möller 1995) rather than cracks.

(3) *Microstructural embrittlement.* The artifact most likely to have undergone brittle fracture owing to microstructural embrittlement is sample number 575 from Hartmann (1970), see figure C.2. Besides fulfilling all the macroscopically-based criteria indicative of brittle fracture, table C.2, this 20k gold disc also contains 0.025 wt. % Pb, which may have embrittled the alloy since the disc's fabrication. Be that as it may, figure 12 and table C.1 show that only eighteen artifacts containing more or less brittle-looking damage were found to have embrittling impurity elements: antimony, lead and bismuth. And one artifact, sample number 119 in Hartmann (1970) was successfully fabricated and is apparently undamaged despite having 0.04 wt. % Te. This is remarkable because tellurium is a potent embrittler of gold: see figure 1 and Okamoto and Massalski (1987) and Raub (1995).

Overall, it seems microstructural embrittlement of high-karat archaeological gold will be very rare, if it occurs at all. This general statement pertains to both fabricated and as-cast artifacts, since the latter are themselves rare, at least in Europe: Hartman's 1970 and 1982 compilations list only four castings (sample numbers 10, 448, 2211 and 3208) out of more than five thousand samples. One might argue that the situation could be different for pre-Columbian goldwork, which is very different in composition and manufacturing technique compared to European gold (La Niece 2000). However, high-karat cast gold also seems to be exceptional in the New World (Furihata 2000).

Archaeological silver embrittlement

There is good evidence for both corrosion-induced and microstructural embrittlement of archaeological silver artifacts (Thompson and Chatterjee 1954; Werner 1965; Ravich 1993; Wanhill *et al.* 1998; Wanhill 1998).

Corrosion-induced embrittlement is partly or mainly due to copper segregation. At low temperatures copper can segregate to grain boundaries, resulting in discontinuous or cellular precipitation (Scharfenberger *et al.* 1972; Gust *et al.* 1978; Schweizer and Meyers 1978) and intergranular corrosion (Werner 1965; Ravich 1993). At high temperatures copper segregates during alloy solidification. This type of segregation results in ambient temperature corrosion that is either interdendritic, in essentially as-solidified microstructures (Scott 1996), or along copper-rich segregation bands (Wanhill 1998). These bands are the remains of solute element

segregation (coring) and interdendritic segregation that have been modified and reduced by mechanical working and annealing.

Microstructural embrittlement appears to be due to lead segregating at low temperatures to grain boundaries (Thompson and Chatterjee 1954; Wanhill *et al.* 1998; Wanhill 1998), at least for the artifacts so far investigated. This attribution is consistent with the compositional data in figure 11, where it is seen that lead is the main impurity in archaeological silver, as pointed out earlier. However, microstructural embrittlement by other impurity elements - notably bismuth – is possible, especially in conjoint action with lead.

Differences between gold and silver: the role of primary solid solubility

From metallurgical knowledge and the chemical compositions and current evidence for microstructural embrittlement of archaeological gold and silver, the most likely embrittling elements are lead, bismuth and antimony, in that order, with arsenic and tellurium less likely.

Table 1 and figure 9 show the primary solid solubilities of lead, bismuth and antimony are much lower in gold than in silver, especially for lead and bismuth. Thus gold is likely to be embrittled only in the as-solidified (cast) condition, with little or no possibility of age-embrittlement. On the other hand, silver is likely to be embrittled also in the aged condition, though not by antimony alone, as mentioned earlier and with reference to sub-table 2.2.

These indicated differences in susceptibility to microstructural embrittlement lead to an essential point. By far the majority of archaeological gold and silver artifacts were mechanically worked and annealed to their final form. As-cast embrittlement could not have been tolerated: the metals would have been reprocessed until ductile. For gold the reprocessing would be expected to eliminate embrittlement. But for silver it is more probable – or even certain (Thompson and Chatterjee 1954; Wanhill *et al.* 1998) – that elimination of as–cast embrittlement need not prevent age-embrittlement.

There remains the assessment of damaged archaeological gold artifacts, notably sample number 575 from Hartmann (1970). This 20k disc contains 0.025 wt. % Pb and its current appearance, see figure C.2, makes it a prime candidate for establishing age-embrittlement of archaeological gold, however unlikely this is.

CONCLUSIONS AND RECOMMENDATIONS

(1) Many impurity or alloying elements could cause microstructural embrittlement of gold and silver. But only lead, bismuth and antimony are likely to be relevant to archaeological gold and silver, especially lead.

(2) As yet there appears to be no good evidence for microstructural embrittlement of high-karat archaeological gold. However, reasonably high purity archaeological silver can suffer age-embrittlement, owing most probably to low temperature segregation of lead to grain boundaries: but see point (4) below.

(3) More than half the damaged archaeological gold artifacts assessed as the likeliest candidates for containing brittle fractures are in the National Museums of Copenhagen and Dublin. Thus it seems feasible to investigate the damaged artifacts at one or both of these locations. Suggestions for investigation are given in Appendix C.3.

(4) Age-embrittlement of archaeological silver should be investigated further. Although lead seems the most likely perpetrator, this has not been established directly.

REFERENCES

Baker, H., and Okamoto H. (eds.), 1992, ASM Handbook, Volume 3, Alloy Phase Diagrams, Section 2, ASM International, Materials Park, Ohio, U.S.A.

Bennett, A., 1994, Technical examination and conservation, Chapter 2 in The Sevso Treasure Part One, Journal of Roman Archaeology, Supplementary Series Number Twelve.

Caley, E.R., 1964, Analysis of Ancient Metals, 36-79, Pergamon Press, Oxford, U.K.

Cope, L.H., 1972, The metallurgical analysis of Roman Imperial silver and *aes* coinage, Methods of Chemical and Metallurgical Investigation of Ancient Coinage (Editors E.T. Hall and D.M. Metcalf), 3-47, Royal Numismatic Society, London, U.K.

Cottrell, A.H., 1988, Introduction to the Modern Theory of Metals, 124-126, The Institute of Metals, London, U.K.

Darken, L.S., and Gurry, R.W., 1953, Physical Chemistry of Metals, 79-90, McGraw-Hill Book Company, New York, New York, U.S.A.

Eluère, C., 1982, Les Ors Préhistoriques, L'Age du Bronze en France 2, Picard, Paris, France.

Ercker, L., 1574, Beschreibung allerfürnemisten mineralischen Ertzt und Berckwerksarten: see translation of Second Edition of 1580 by A.G. Sisco and C.S. Smith, 1951, Lazarus Ercker's Treatise on Ores and Assaying, 80-81, 191-198, University of Chicago Press, Chicago, Illinois, U.S.A.

Furihata, J., 2000, Technical examination of Columbian gold objects, The Getty Conservation Institute, Los Angeles, California, U.S.A.

Gale, N.H., and Stos-Gale, Z.A., 1981a, Ancient Egyptian silver, Journal of Egyptian Archaeology, 67, 103-115.

Gale, N.H., and Stos-Gale, Z.A., 1981b, Lead and silver in the ancient Aegean, Scientific American, 244, 142-152.

Gordus, A.A., 1972, Neutron activation analysis of coins and coin-streaks, Methods of Chemical and Metallurgical Investigation of Ancient Coinage (Editors E.T. Hall and D.M. Metcalf), 127-148, Royal Numismatic Society, London, U.K.

Gordy, W, and Thomas, W.J.O., 1956, Electronegativities of the elements, Journal of Chemical Physics, 24, 439-444.

Gowland, W., 1918, Silver in Roman and earlier times: I. Pre-historic and proto-historic times, Archaeologia, 69, 121-160.

Graf, L., 1947, Die Ursache der Spannungskorrosionsempfindlichkeit homogener Legierungen, Zeitschrift für Metallkunde, 38, 193-207.

Graf, L., and Budke, J., 1955, Zum Problem der Spannungskorrosion homogener Mischkristalle III. Abhängigkeit der Spannungskorrosions-Empfindlichkeit von Kupfer-Gold- und Silber-Gold-Mischkristallen vom Goldgehalt und Zusammenhang mit dem "Mischkristall-Effekt", Zeitschrift für Metallkunde, 46, 378-385.

Gschneider, K.A., Jr., 1980, L.S. (Larry) Darken's contributions to the theory of alloy formation and where we are today, Theory of Alloy Phase Formation (Editor L.H. Bennett), 1-34, The Metallurgical Society of AIME, Warrendale, Pennsylvania, U.S.A.

Gust, W., Predel, B., and Diekstall, K., 1978, Zur diskontinuierlichen Ausscheidung in Silber -6,2 At. % - Kupfer-Dreikristallen, Zeitschrift für Metallkunde, 69, 75-80.

Hartmann, A., 1970, Prähistorische Goldfunde aus Europa. Studien zu den Anfängen der Metallurgie 3, Gebr. Mann Verlag, Berlin, Germany.

Hartmann, A., 1982, Prähistorische Goldfunde aus Europa II. Studien zu den Anfängen der Metallurgie 5, Gebr. Mann Verlag, Berlin, Germany.

Hatchett, C., 1803, Experiments and observations on the various alloys, on the specific gravity, and on the comparative wear of gold, Philosophical Transactions of the Royal Society of London, Part 1, 43-194.

Hauptmann, A., Rehren, Th., and Pernicka, E., 1995, The composition of gold from the ancient mining district of Verespatak/Roşia Montană, Romania, Prehistoric Gold in Europe: Mines, Metallurgy and Manufacture (Editors G. Morteani and J.P. Northover), 369-381, Kluwer Academic Publishers, Dordrecht, The Netherlands.

Hawkes, S.C., Merrick, J.M., and Metcalf, D.M., 1966, X-ray fluorescent analysis of some Dark Age coins and jewellery, Archaeometry, 9, 98-138.

Hondros, E.D., and Seah, M.P., 1977, Segregation to interfaces, International Metallurgical Reviews, 22, 262-301.

Hondros, E.D., Seah, M.P., Hofmann, S., and Lejček, P., 1996, Chapter 13 in Physical Metallurgy, Fourth Edition, Volume II (Editors R.W. Cahn and P. Haasen), Elsevier Science B.V., Amsterdam, The Netherlands.

Hultgren, R., Desai, P.D., Hawkins, D.T., Gleiser, M., Kelley, K.K., and Wagman, D.D., 1973, Selected Values of the Thermodynamic Properties of the Elements, American Society for Metals (ASM), Metals Park, Ohio, U.S.A.

Hume-Rothery, W., and Raynor, G.V., 1954, The Structure of Metals and Alloys, Third Edition, 100-108, 126-132, 194-210, The Institute of Metals, London, U.K.

Jones, H., 1937, The phase boundaries in binary alloys, part 2: the theory of the α, β phase boundaries, Proceedings of the Physical Society of London, 49, 250-257.

King, H.W., 1965, Structure of the pure metals, Chapter 2 in Physical Metallurgy (Editor R.W. Cahn), North-Holland Publishing Company, Amsterdam, The Netherlands.

La Niece, S., 2000, Personal Communication from the Department of Scientific Research, The British Museum, London, U.K.

Lehrberger, G., and Raub, Ch.J., 1995, A look into the interior of Celtic gold coins, Prehistoric Gold in Europe: Mines, Metallurgy and Manufacture (Editors G. Morteani and J.P. Northover), 341-355, Kluwer Academic Publishers, Dordrecht, The Netherlands.

Logan, H.L., (1966), The Stress Corrosion of Metals, 256, John Wiley and Sons, Inc., New York, New York, U.S.A.

Lucas, A., 1928, Silver in ancient times, Journal of Egyptian Archaeology, 14, 313-319.

MacDowall, D.W., 1972, The Pre-Mohammedan coinage of Greater India: a preliminary list of some analyses, Methods of Chemical and Metallurgical Investigation of Ancient Coinage (Editors E.T. Hall and D.M. Metcalf), 371-381, Royal Numismatic Society, London, U.K.

Massalski, T.B., 1996, Chapter 3 in Physical Metallurgy, Fourth Edition, Volume I (Editors R.W. Cahn and P. Haasen), Elsevier Science B.V., Amsterdam, The Netherlands.

Massalski, T.B., Murray, J.L., Bennett, L.H., Baker, H., and Kacprzak, L. (eds.), 1986, Binary Alloy Phase Diagrams, Volume 1, 35, 43, 44, 59, 60, 303-305, American Society for Metals (ASM), Metals Park, Ohio, U.S.A.

McKerrell, H., and Stevenson, R.B.K., 1972, Some analyses of Anglo-Saxon and associated Oriental silver coinage, Methods of Chemical and Metallurgical Investigation of Ancient Coinage (Editors E.T. Hall and D.M. Metcalf), 195-209, Royal Numismatic Society, London, U.K.

Meeks, N.D., and Tite, M.S., 1980, The analysis of platinum-group element inclusions in gold antiquities, Journal of Archaeological Science, 7, 267-275.

Metcalf, D.M., 1972, Analyses of the metal contents of Medieval coins, Methods of Chemical and Metallurgical Investigation of Ancient Coinage (Editors E.T. Hall and D.M. Metcalf), 383-434, Royal Numismatic Society, London, U.K.

Möller, P., 1995, Electrochemical corrosion of natural gold alloys, Prehistoric Gold in Europe: Mines, Metallurgy and Manufacture (Editors G. Morteani and J.P. Northover), 357-367, Kluwer Academic Publishers, Dordrecht, The Netherlands.

Oddy, W.A., and La Niece, S., 1986, Byzantine gold coins and jewellery, Gold Bulletin, 19, 19-27.

Ogden, J.M., 1977, Platinum group metal inclusions in ancient gold artefacts, Journal of the Historical Metallurgical Society, 11, 53-72.

Okamoto, H., and Massalski, T.B., 1987, Phase Diagrams of Binary Gold Alloys, 298-305, ASM International, Metals Park, Ohio, U.S.A.

Pauling, L., 1945, The Nature of the Chemical Bond, Second Edition, 58-75, Cornell University Press, Ithaca, New York, U.S.A.

Pauling, L., 1947, Atomic radii and interatomic distances in metals, Journal of the American Chemical Society, 69, 542-553.

Perea, A., and Rovira, S., 1995, The gold from Arrabalde, Prehistoric Gold in Europe: Mines Metallurgy and Manufacture (Editors G. Morteani and J.P. Northover), 471-490, Kluwer Academic Publishers, Dordrecht, The Netherlands.

Pettifor, D.G., 1984, A chemical scale for crystal-structure maps, Solid State Communications, 51, 31-34.

Pettifor, D.G., 1988, Structure maps for pseudobinary and ternary phases, Materials Science and Technology, 4, 675-691.

Philip, G., and Rehren, T., 1996, Fourth millenium BC silver from Tell esh-Shuna, Jordan: archaeometallurgical investigation and some thoughts on ceramic skeuomorphs, Oxford Journal of Archaeology, 15, 129-150.

Pingel, V., 1995, Technical aspects of prehistoric gold objects on the basis of material analyses, Prehistoric Gold in Europe: Mines, Metallurgy and Manufacture (Editors G. Morteani and J.P. Northover), 385-398, Kluwer Academic Publishers, Dordrecht, The Netherlands.

Prince, A., Raynor, G.V., and Evans, D.S., 1990, Phase Diagrams of Ternary Gold Alloys, 7-42, 47-52, The Institute of Metals, London, U.K.

Pugh, E.N., Craig, E.V., and Sedriks, A.J., 1969, The stress-corrosion cracking of copper, silver and gold alloys, Proceedings of Conference: Fundamental Aspects of Stress Corrosion Cracking (Editors R.W. Staehle, A.J. Forty and D. van Rooyen), National Association of Corrosion Engineers, Houston, Texas, U.S.A.

Raub, Ch.J., 1995, The metallurgy of gold and silver in prehistoric times, Prehistoric Gold in Europe: Mines, Metallurgy and Manufacture (Editors G. Morteani and J.P. Northover), 243-259, Kluwer Academic Publishers, Dordrecht, The Netherlands.

Ravich, I.G., 1993, Annealing of brittle archaeological silver: microstructural and technological study, in 10th Triennial Meeting of the International Council of Museums Committee for Conservation, Preprints of the Seminar: August 22/27, 1993, II, 792-795, Washington, D.C., U.S.A.

Roberts-Austen, W.C., 1888, On certain mechanical properties of metals considered in relation to the Periodic Law, Philosophical Transactions of the Royal Society of London, A179, 339-350.

Scharfenberger, W., Schmitt, G., and Borchers, H., 1972, Über die Kinetik der diskontinuierlichen Ausscheidung der Silberlegierung mit 7,5 Gew. - % Cu, Zeitschrift für Metallkunde, 63, 553-560.

Schweizer, F., and Meyers, P., 1978, Authenticity of ancient silver objects: a new approach, MASCA Journal, 1, 9-10.

Scott, D.A., 1996, Technical study of a ceremonial Sican tumi figurine, Archaeometry, 38, 305-311.

Seah, M.P., 1980a, Adsorption-induced interface decohesion, Acta Metallurgica, 28, 955-962.

Seah, M.P., 1980b, Chemistry of solid - solid interfaces – A review of its characterization, theory, and relevance to materials science, Journal of Vacuum Science and Technology, 17, 16-24.

Shewmon, P.G., 1998, Grain boundary cracking, Metallurgical and Materials Transactions A, 29A, 1535-1544.

Smith, C.S., 1965, The interpretation of microstructures of metallic artifacts, in Application of Science in Examination of Works of Art (Editor W.J. Young), 20-52, Boston Museum of Fine Arts, Boston, Massachusetts, U.S.A.

Taylor, J.J., 1980, Bronze Age Goldwork in the British Isles, Cambridge University Press, Cambridge, U.K.

Teatum, E.T., Gschneider, K.A., Jr., and Waber, J.T., 1968, Compilation of calculated data useful in predicting metallurgical behavior of the elements in binary alloy systems, Los Alamos Scientific Laboratory Report LA-4003, Clearing House for Federal Scientific and Technical Information, Springfield, Virginia, U.S.A.

Thompson, A.W., and Knott, J.F., 1993, Micromechanisms of brittle fracture, Metallurgical Transactions A, 24A, 523-534.

Thompson, F.C., and Chatterjee, A.K., 1954, The age-embrittlement of silver coins, Studies in Conservation, 1, 115-126.

Tylecote, R.F., 1986, The Prehistory of Metallurgy in the British Isles, 3-4, 54-61, The Institute of Metals, London, U.K.

Tylecote, R.F., 1987, The Early History of Metallurgy in Europe, 69-80, 138-140, 280-290, Longman Inc., New York, New York, U.S.A.

Tylecote, R.F., 1992, A History of Metallurgy, Second Edition, 71, The Institute of Materials, London, U.K.

Waber, J.T., Gschneider, K.A., Jr., Larson, A.C., and Prince, M.Y., 1963, Prediction of solid solubility in metallic alloys, Transactions of the Metallurgical Society of AIME, 227, 717-723.

Waldhauser, J., 1995, Celtic gold in Bohemia, Prehistoric Gold in Europe: Mines, Metallurgy and Manufacture (Editors G. Morteani and J.P. Northover), 577-596, Kluwer Academic Publishers, Dordrecht, The Netherlands.

Wanhill, R.J.H., 1998, Brittle archaeological silver. Identification, restoration and conservation, NLR Technical Publication 97647 L, National Aerospace Laboratory NLR, Amsterdam, The Netherlands. Also: Materialen, 2000, 16, 30-35.

Wanhill, R.J.H., Steijaert, J.P.H.M., Leenheer, R., and Koens, J.F.W., 1998, Damage assessment and preservation of an Egyptian silver vase (300-200 BC), Archaeometry, 40, 123-137.

Werner, A.E., 1965, Two problems in the conservation of antiquities: corroded lead and brittle silver, in Application of Science in Examination of Works of Art (Editor W.J. Young), 96-104, Boston Museum of Fine Arts, Boston, Massachusetts, U.S.A.

Table 1 Selected metallic and semi-metallic element properties

ELEMENT	ATOMIC NUMBER	EMPIRICAL ORDERING NUMBER	ATOMIC DIAMETER (nm)	PAULING ATOMIC DIAMETER, C.N.12 (nm)	ALLOYING ELEMENT PRIMARY SOLID SOLUBILITY LIMIT				ELECTRO-NEGATIVITY $(eV)^{1/2}$	NUMBER OF VALENCE ELECTRONS	SUBLIMATION ENTHALPY (J/m^2)
					IN GOLD		IN SILVER				
					wt.%	at.%	wt.%	at.%			
Li	3	12	0.3456	0.3098	0.7	16.7	9.1	60.9	0.95	1	3.37
Na	11	11	0.4226	0.3792	0	0	0	0	0.95	1	1.53
Al	13	80	0.3164	0.2858	2.0	13.0	6.1	20.6	1.52	3	8.34
K	19	10	0.5236	0.4698	0	0	0	0	0.83	1	0.84
Mn	25	60	0.2856	0.2522;0.2612	11.0	30.7	31	47	2.24;1.92	7;5	8.83
Cu	29	72	0.2826	0.2552	100	100	8.8	14.1	1.82	1	10.7
Zn	30	76	0.3076	0.2758	14.0	32.9	29.0	40.3	1.66	2	3.50
Ga	31	81	0.3344	0.2816	4.8	12.5	12.0	17.4	1.80	3	6.19
Ge	32	84	0.3510	0.2732	1	2.7	6.7	9.6	1.90	4	7.70
As	33	89	0.3452	0.2780	0	0	5.5	7.7	2.08	5	6.46
Se	34	93	0.3726	0.280	0	0	0	0	2.46	6	3.79
Rb	37	9	0.5600	0.4960	0	0	0	0	0.83	1	0.67
Rh	45	65	0.2974	0.2684	0.84	1.6	0	0	2.20	9	15.9
Pd	46	69	0.3042	0.2746	100	100	100	100	2.21	10	10.4
Ag	47	71	0.3196	0.2884	100	100	100	100	1.68	1	7.09
Cd	48	75	0.3452	0.3086	21.6	32.6	43.2	42.2	1.58	2	2.40
In	49	79	0.3682	0.3320	7.8	12.7	22.1	21.1	1.82	3	4.58
Sn	50	83	0.3724	0.3084;0.3240	4.3	7.0	12.5	11.5	1.83;1.65	4;2	5.55
Sb	51	88	0.3864	0.3180	0.75	1.2	8.1	7.2	1.98	5	4.52
Te	52	92	0.4010	0.320	0.10	0.15	0	0	1.92	6	3.12
Au	79	70	0.3188	0.2878	100	100	100	100	1.90	1	9.25
Tl	81	78	0.3784	0.3424	1.04	1.00	13.8	7.8	1.86	3	3.24
Pb	82	82	0.3898	0.3492	0.12	0.11	5.2	2.8	1.93	4	3.29
Bi	83	87	0.4072	0.340	0	0	4.9	2.6	1.86	5	3.23

(1) Empirical ordering number acknowledges chemical similarity of elements from the same Group of the Periodic Table (Pettifor 1988).

(2) Atomic diameters from King (1965) and Pauling (1947). The latter depend on the number of nearest neighbour atoms (coordination number, C.N.) for each atom in solid solution in the matrix. C.N.=12 for atoms in solid solution in gold and silver.

(3) Primary solid solubility limits from Baker *et al.* (1992) and Massalski *et al.* (1986).

(4) Electronegativities and number of valence electrons from Teatum *et al.* (1968).

(5) Sublimation enthalpies (per unit area) according to Seah (1980a) using Hultgren *et al.* (1973).

Table 2 Gold and silver binary alloys with alloying element low primary solid solubility: PSSL = Primary Solid Solubility Limit; max = maximum; eut = eutectic temperature; amb = ambient temperatures. Data (phase diagrams) from Baker et al. (1992), see Appendix A, and Thompson and Chatterjee (1954)

2.1 Zero or very low PSSL

BINARY ALLOY SYSTEMS	DILUTE ALLOY PHASE DIAGRAM CHARACTERISTICS	EQUILIBRIUM PHASES AT AMBIENT TEMPERATURES		REMARKS
		PRIMARY CRYSTALS/GRAINS	BETWEEN PRIMARY CRYSTALS/GRAINS	
Au-As	Au-As eutectic, 56.6 at.% As, 636°C	Au	eutectic Au+As	
Au-Bi	Au-Au_2Bi peritectic, 371°C	Au	Au_2Bi	$Au_2Bi \rightarrow Au+Bi$ below 116°C?
Au-K	Au-Au_5K eutectic, 7.1 at.% K, 975°C	Au	eutectic Au+Au_5K	
Au-Na	Au-Au_2Na eutectic, 16.8 at.% Na, 875°C	Au	eutectic Au+Au_2Na	Au_5Na formation below 800°C?
Au-Rb	Au-Au_5Rb peritectic, 730°C	Au	Au_5Rb	
Au-Se	monotectics, 963°C and 760°C; Au-AuSe peritectic, 425°C	Au	AuSe	
Au-Pb	Au-Au_2Pb peritectic, 434°C	α,max.0.11 at.% Pb	Au_2Pb	
Au-Te	Au-$AuTe_2$ eutectic, 52.5 at.% Te, 447°C	α,max.0.10 at.% Te	eutectic Au+$AuTe_2$	
Ag-K	phase diagram not available (Massalski *et al.* 1986)	Ag		
Ag-Na	Ag-Ag_2Na peritectic, 322°C?; Ag-Na eutectic, > 99.9 at.% Na, 97.7°C	Ag	Na or possibly Ag_2Na	
Ag-Rb	phase diagram not available (Massalski *et al.* 1986)	Ag		
Ag-Se	monotectic, 890°C; Ag-Ag_2Se eutectic, 12.1 at.% Se, 840°C	Ag	eutectic Ag+Ag_2Se	
Ag-Te	Ag-Ag_2Te eutectic, 11.5 at.% Te, 869°C	Ag	eutectic Ag+Ag_2Te	

CONTINUED ON NEXT PAGE

Table 2 CONTINUED FROM PREVIOUS PAGE

2.2 $PSSL_{max}$ at eutectic or peritectic temperatures

BINARY ALLOY SYSTEMS	DILUTE ALLOY PHASE DIAGRAM CHARACTERISTICS	ALLOYING ELEMENT		EQUILIBRIUM PHASES AT AMBIENT TEMPERATURES		
				PRIMARY CRYSTALS/GRAINS		BETWEEN PRIMARY CRYSTALS/GRAINS
		$PSSL_{max}$ (at.%)	$PSSL_{amb}$ (at.%)	ALLOYS BELOW $PSSL_{amb}$	ALLOYS ABOVE $PSSL_{amb}$	ALLOYS ABOVE $PSSL_{max}$
Au-Ge	α-Ge eutectic, 28.0 at.% Ge, 361°C	2.7	0		α→Au+Ge	Au+Ge from eutectic α+Ge
Au-Sn	α-$Au_{10}Sn$ peritectic (up to 9.1 at.% Sn), 532°C; possible eutectoids at 245°C and 60°C	7.0	~3?	α	α→α+(α+Au_5Sn)	eutectoid α+Au_5Sn
Ag-As	α-ζ peritectic (up to 10.1 at.% As), 582°C; eutectoid, 446°C	7.7	~2?	α	α→α+As	eutectoid α+As
Ag-Ge	α-Ge eutectic, 24.2 at.% Ge, 651°C	9.6	~0		α→Ag+Ge	Ag+Ge from eutectic α+Ge
Ag-Sb	α-ζ peritectic (up to 8.8 at.% Sb), 702.5°C	7.2	~4	α	α→α+ζ	ζ (intermediate phase)
Ag-Sn	α-ζ peritectic (up to 12.9 at.% Sn), 724°C	11.5	~9	α	α→α+ζ	ζ (intermediate phase)

2.3 $PSSL_{max} > PSSL_{eut}$

BINARY ALLOY SYSTEMS	DILUTE ALLOY PHASE DIAGRAM CHARACTERISTICS	ALLOYING ELEMENT			EQUILIBRIUM PHASES AT AMBIENT TEMPERATURES		
					PRIMARY CRYSTALS/GRAINS		BETWEEN PRIMARY CRYSTALS/GRAINS
		$PSSL_{max}$ (at.%)	$PSSL_{eut}$ (at.%)	$PSSL_{amb}$ (at.%)	ALLOYS BELOW $PSSL_{amb}$	ALLOYS ABOVE $PSSL_{amb}$	ALLOYS ABOVE $PSSL_{eut}$
Au-Sb	α-$AuSb_2$ eutectic, 35.5 at.% Sb, 360°C	1.2	~0.8	0		α→Au+Sb	Au+$AuSb_2$ from eutectic α+$AuSb_2$
Au-Tl	α-Tl eutectic, 75.3 at.% Tl, 147°C	1.0	0	0		α→Au+Tl	eutectic Au+Tl
Ag-Bi	α-Bi eutectic, 95.3 at.% Bi, 262.5°C	2.6	0.83	~0		α→Ag+Bi	Ag+Bi from eutectic α+Bi
Ag-Pb	α-Pb eutectic, 95.5 at.% Pb, 304°C	2.8	0.79	<0.05	α	α→α+Pb	α+Pb from eutectic α+Pb
Ag-Tl	α-Tl eutectic, 97.4 at.% Tl, 291°C	7.8	5.1	?	α	α→α+Tl	α+Tl from eutectic α+Tl

Table 3 Classifications of impurity elements in native gold and processed archaeological gold artifacts, concentrating on the actually or potentially embrittling elements tin, lead, bismuth, antimony, arsenic and tellurium

3.1 Numbers of analyses and impurity detections

IMPURITY ELEMENT CLASSIFICATIONS	85 ≤ Au wt.% < 95						95 ≤ Au wt.%						REFERENCES AND COMMENTS
	Sn	Pb	Bi	Sb	As	Te	Sn	Pb	Bi	Sb	As	Te	
NATIVE GOLD		29 ANALYSES						11 ANALYSES					Tylecote (1986,1987)
trace : < 0.1 wt.%	3	2			1			1	1	1			Hg 8/1; Pt 1/0
minor : 0.1-0.5 wt.%													Hg 0/1; Pt 1/0
minor→ main : > 0.5 wt.%								1	1				Hg 2/0
ARTIFACTS		478 ANALYSES						30 ANALYSES					Hartmann (1970)
trace : < 0.1 wt.%	265	13	1			1	12	1	1				Hg 3/0; Pt 19/7
minor : 0.1-0.5 wt.%	130	1					2						Pt 1/0
minor→ main : > 0.5 wt.%	7												Sn = 1.8 wt.% maximum
ARTIFACTS		1173 ANALYSES						104 ANALYSES					Hartmann (1982)
trace : < 0.1 wt.%	585	28	28	14	1		38	8	1	1	1		Hg 10/8; Pt 104/40
minor : 0.1-0.5 wt.%	360	1					11						Pt 3/1
minor→ main : > 0.5 wt.%	13												Sn = 1.3 wt.% maximum

3.2 Numbers of detections and wt.% of lead, bismuth, antimony, arsenic and tellurium in artifacts (Hartmann 1970, 1982)

IMPURITY ELEMENT CLASSIFICATIONS	85 ≤ Au wt.% < 95					95 ≤ Au wt.%			
	Pb	Bi	Sb	As	Te	Pb	Bi	Sb	As
trace	41:≤0.07	29:<0.01	14:<0.01	1:<0.01	1:0.04	9:≤0.09	2:<0.01	1:<0.01	1:0.04
minor	2:0.24,0.32								

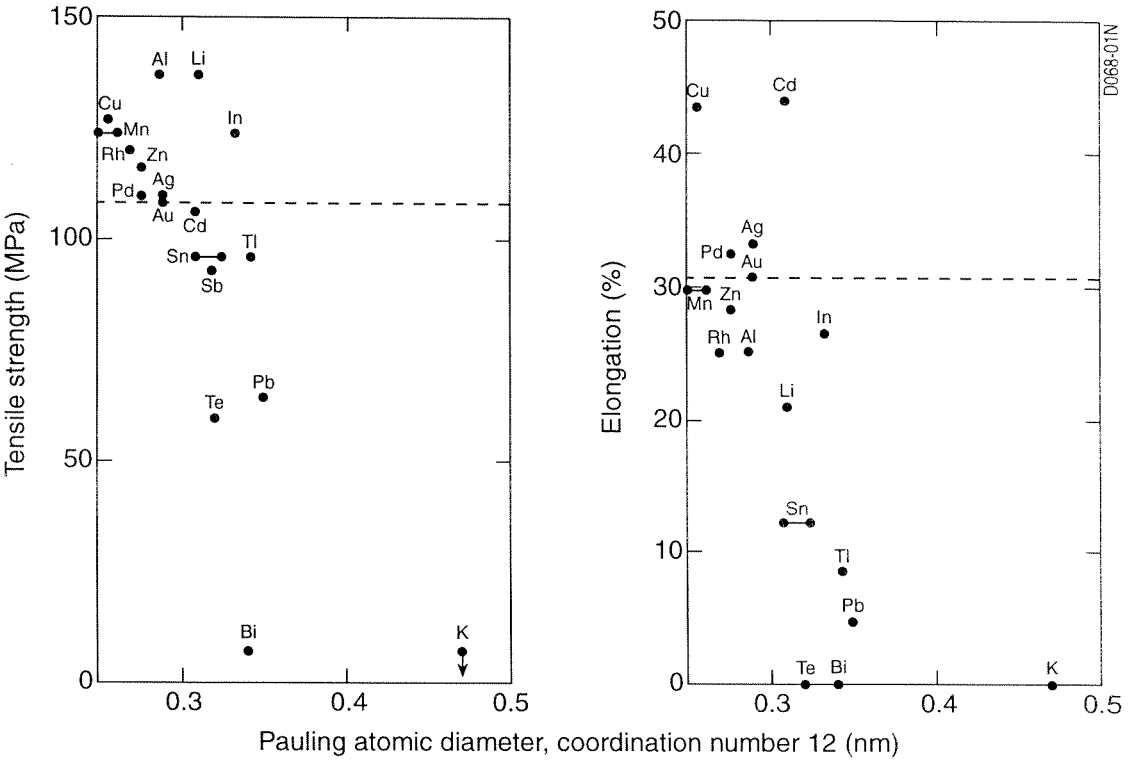

Fig. 1 Tensile strength and elongation of cast Au - 0.2 wt. % alloys versus alloying element atomic diameters in solid solution. Mechanical property data from Roberts-Austen (1888), atomic diameters from table 1

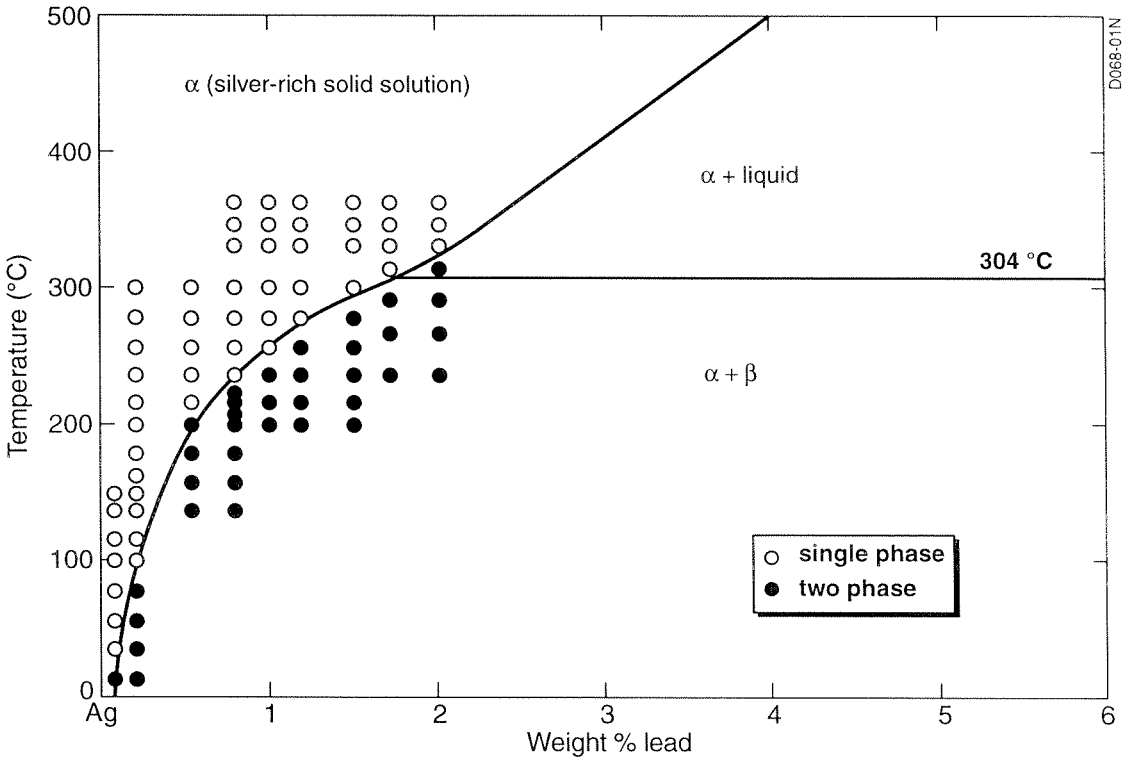

Fig. 2 Silver-rich low temperature region of the Ag-Pb equilibrium phase diagram, determined by ageing supersaturated solid solutions at the indicated temperatures (Thompson and Chatterjee 1954)

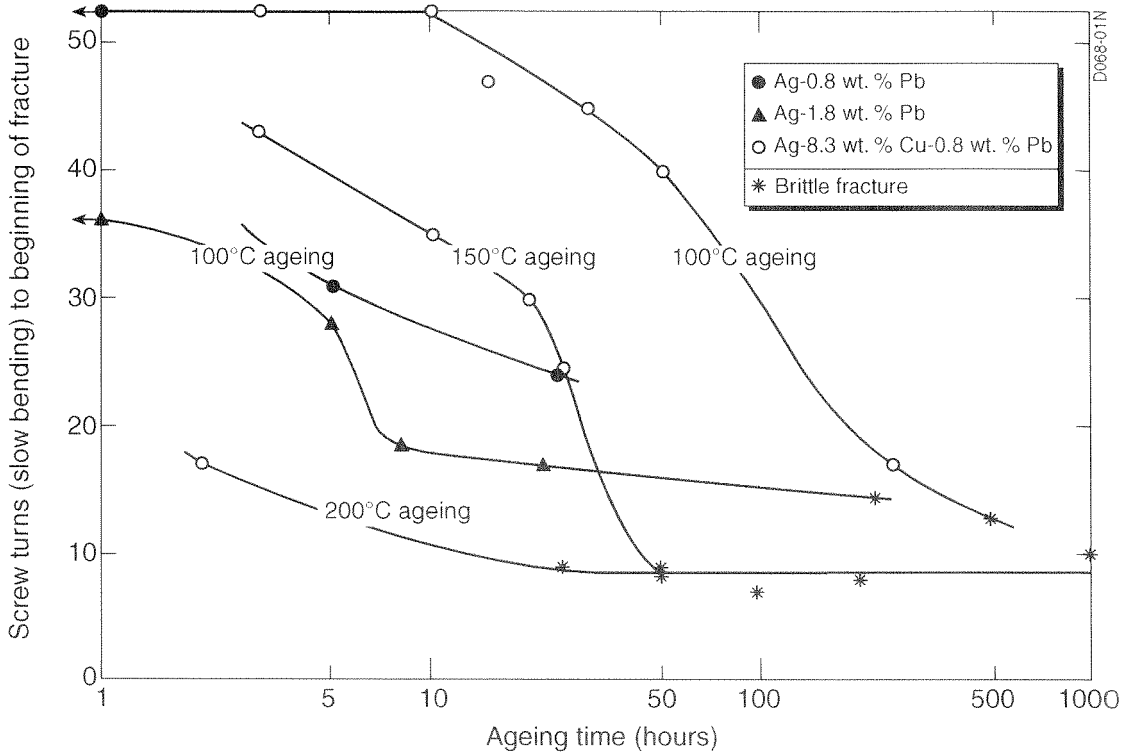

Fig. 3 Age-embrittlement of cast, solution treated and aged Ag-Pb and Ag-Cu-Pb alloys. Data from Thompson and Chatterjee (1954)

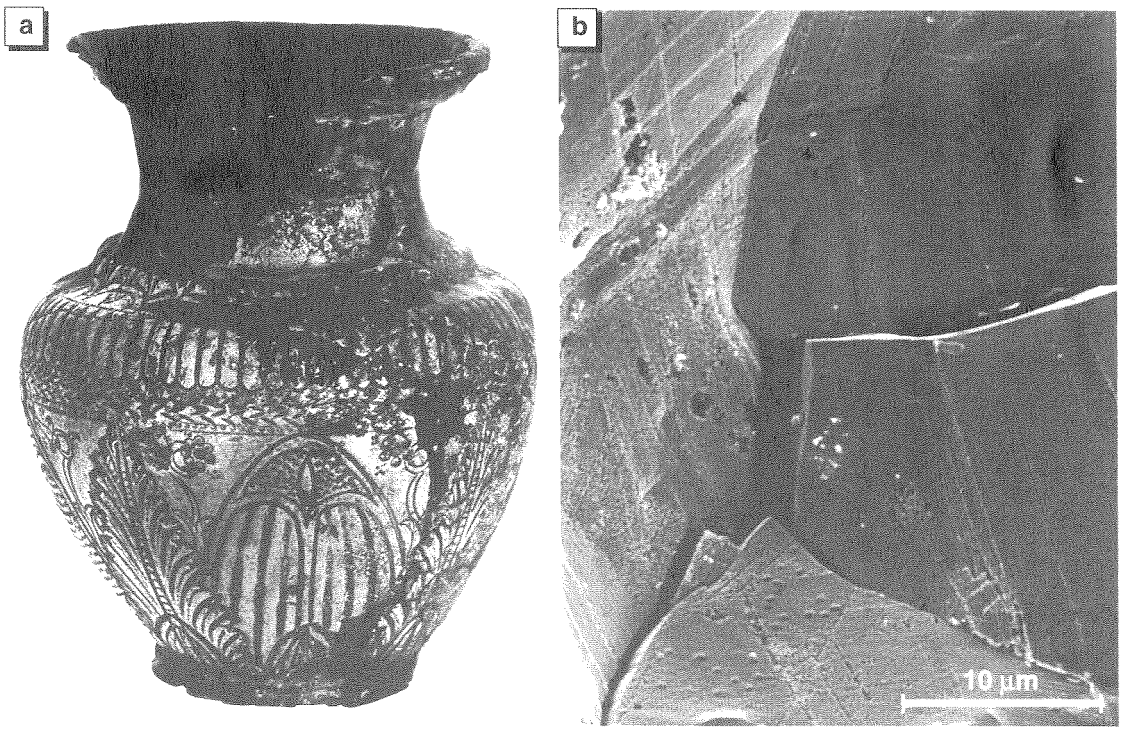

Fig. 4 Brittle grain boundary fracture in a sample from an Egyptian silver vase (Wanhill et al. 1998)

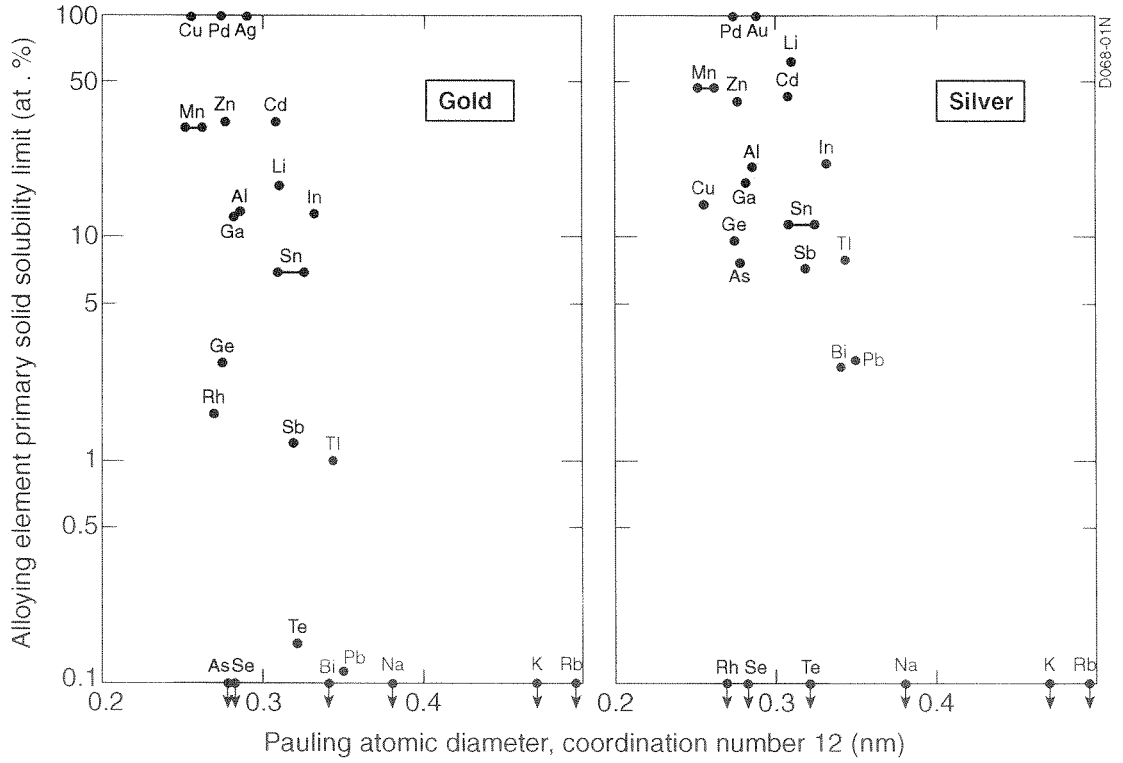

Fig. 5 Application of the size-factor rule to solid solutions in gold and silver. The shaded regions show the ranges of favourable size-factor, bounded by the limits ±15% of the atomic diameters of gold and silver. Data from table 1

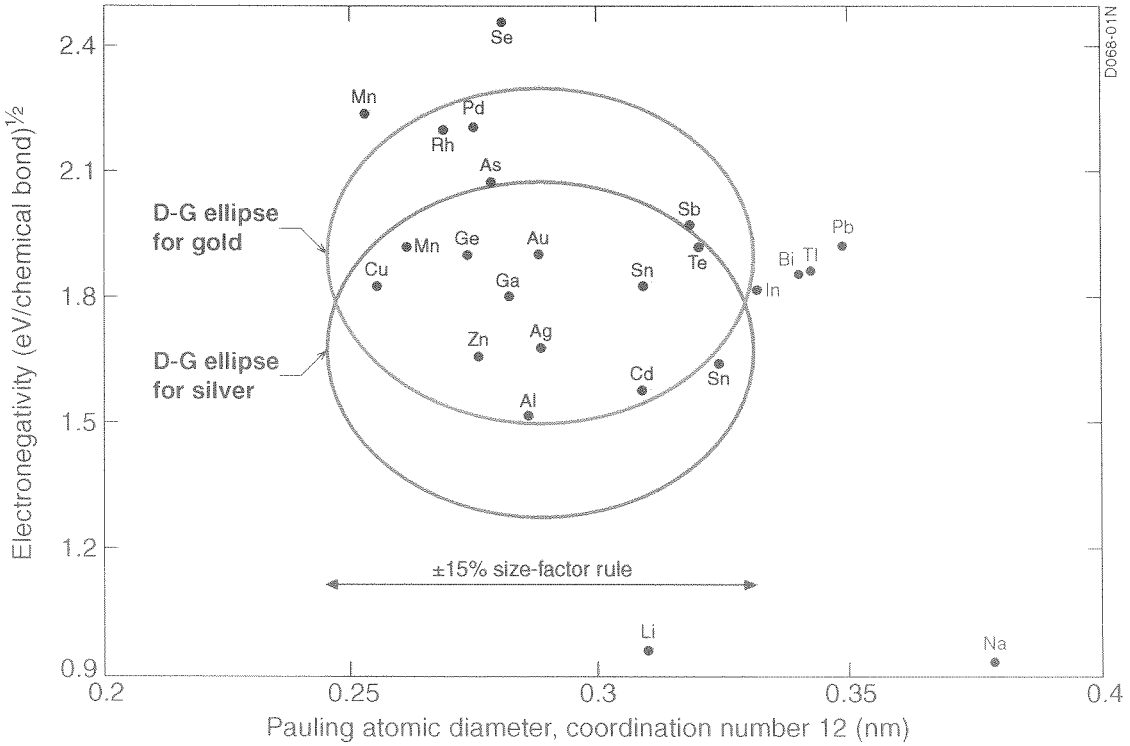

Fig. 6 Darken-Gurry (D-G) maps for solid solutions in gold and silver. Solute elements within the ellipse boundaries, minor axes ±0.4 (eV)$^{1/2}$, are predicted to have solid solubilities greater than 5-10 at . % . Data from table 1

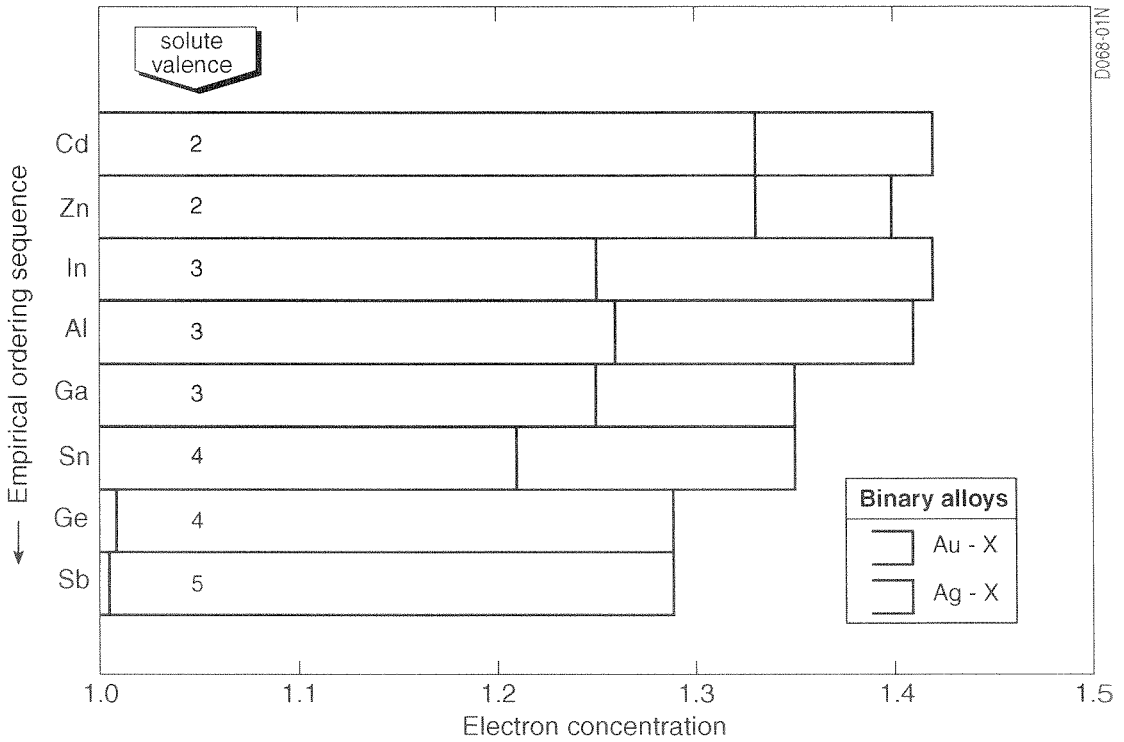

Fig. 7 B-subGroup alloying element primary solid solubility limits in gold and silver, expressed as electron concentrations. The electron concentration is given by [V(100-PSSL)+vPSSL]/100, where PSSL is the primary solid solubility limit in at. % and V and v are the number of valence electrons of the solvent and solute respectively. Data from table 1

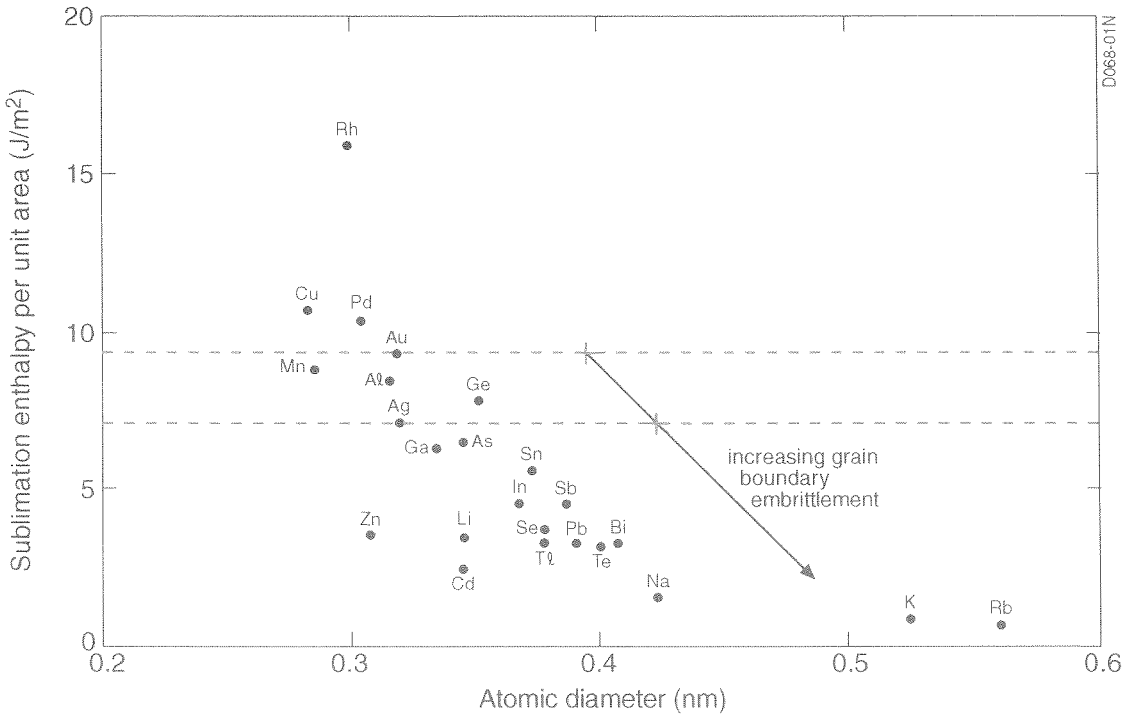

Fig. 8 Embrittlement plot for matrix (Au, Ag) and segregant elements. After Seah (1980a), data from table 1

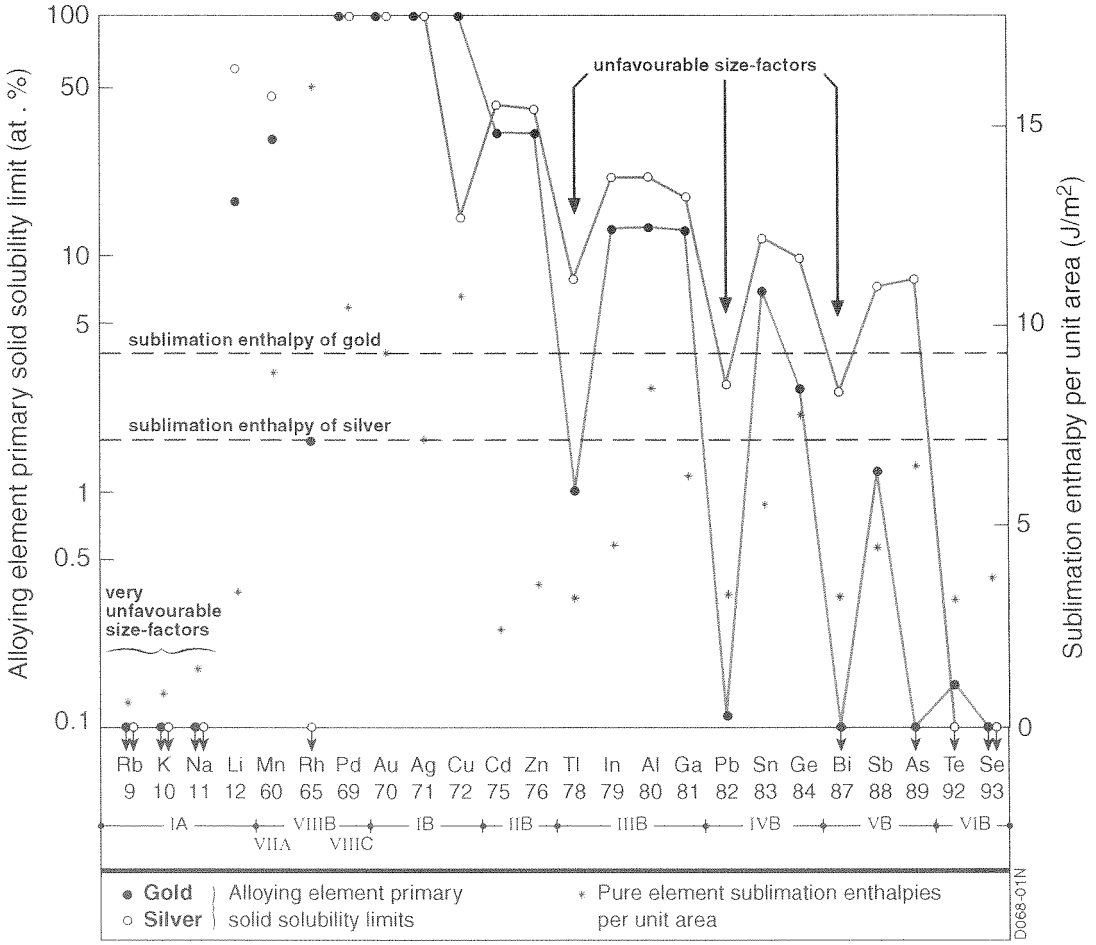

Fig. 9 Correlations between alloying element primary solid solubility limits in gold and silver and the pure element sublimation enthalpies per unit area. The numerical sequence of the elements is the empirical ordering due to Pettifor (1988). The shaded regions denote the matrix and alloying element combinations that would seem most likely to result in segregation-induced grain boundary fracture under equilibrium conditions (see text). Data from table 1

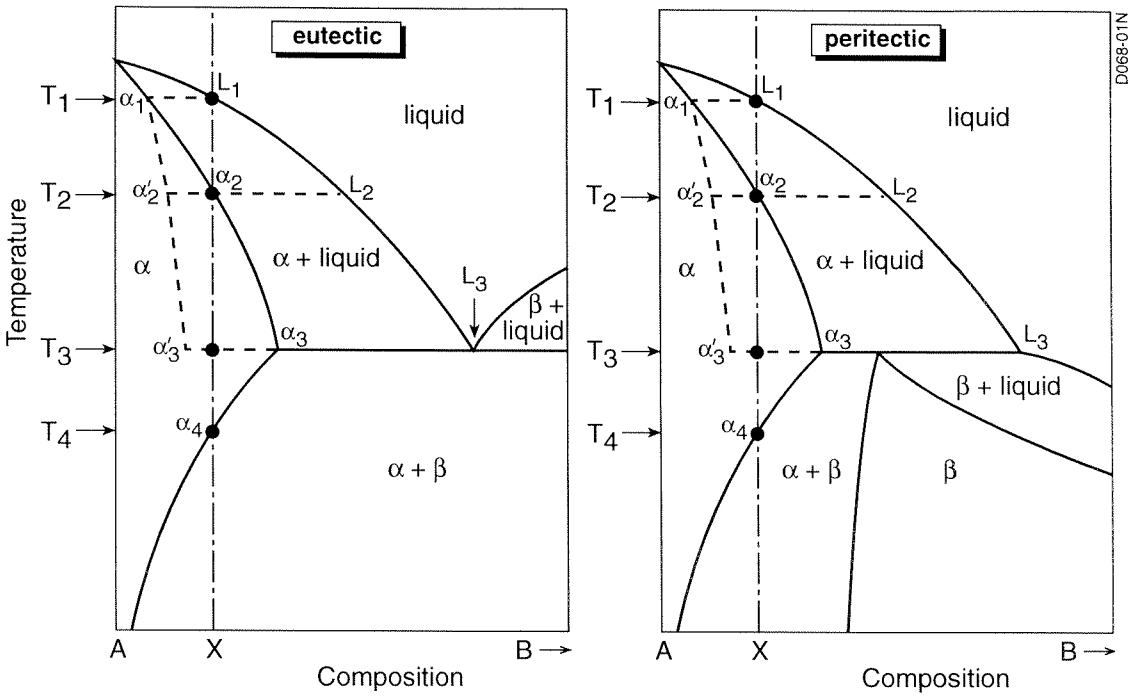

Fig. 10 Schematic binary alloy equilibrium phase diagrams involving eutectic or peritectic reactions and illustrating the effect of non-equilibrium cooling on solidification of dilute alloys of bulk composition X (see text)

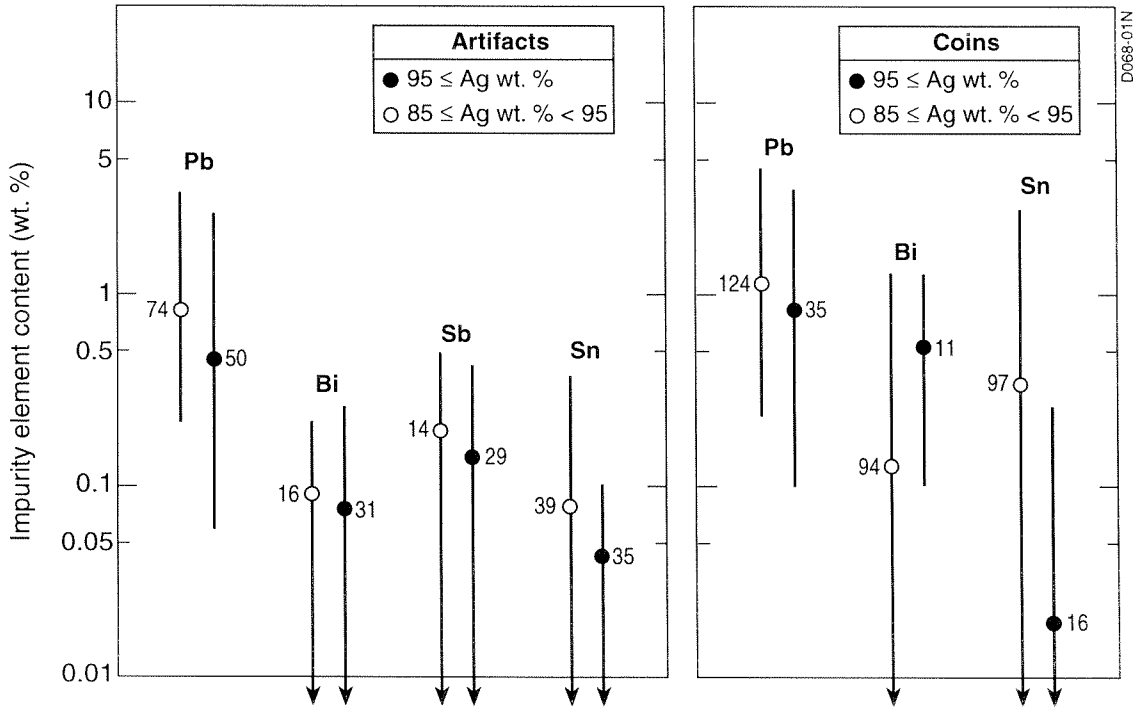

Fig. 11 Actually or potentially embrittling impurity elements in archaeological silver artifacts and coins. Data from Lucas (1928), Caley (1964), Cope (1972), Gordus (1972), MacDowall (1972), McKerrell and Stevenson (1972), Metcalf (1972), Gale and Stos-Gale (1981a), Tylecote (1992), Bennett (1994) and Perea and Rovira (1995), see Appendix B

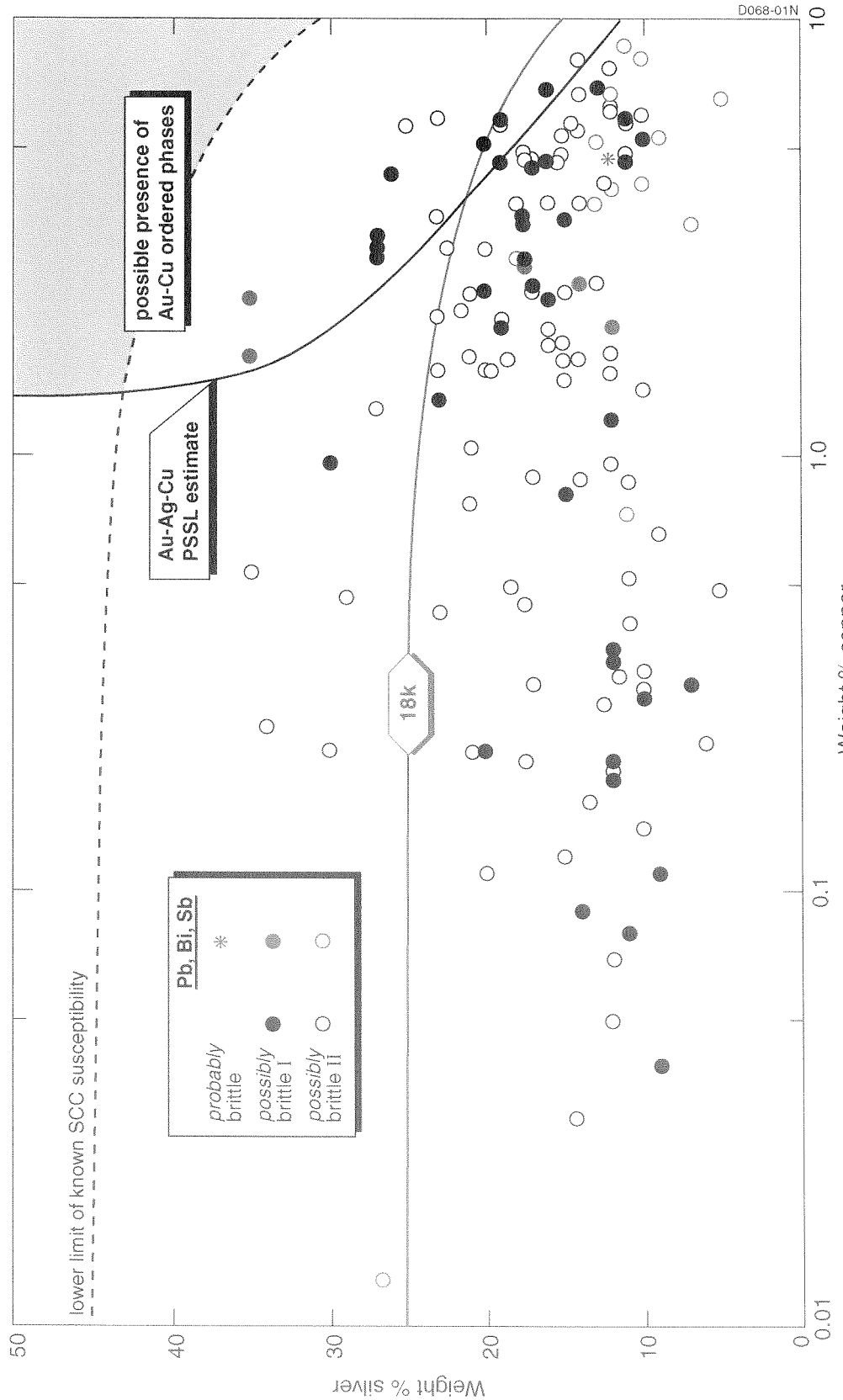

Fig. 12 Archaeological gold artifacts illustrated in Hartmann (1970, 1982) and containing tears or cracks, plotted on a silver-copper compositional diagram. The PSSL (Primary Solid Solubility Limit) is derived from Prince et al. (1990). The lower limit of SCC (Stress Corrosion Cracking) susceptibility is derived from Graf (1947), Graf and Budke (1955), Logan (1966) and Pugh et al. (1969). The artifact data are given in Appendix C.1

This page is intentionally left blank.

Appendix A Gold and silver binary alloy equilibrium phase diagrams in support of table 2

A.1 Atomic weights

ELEMENT	SYMBOL	ATOMIC WEIGHT*	ELEMENT	SYMBOL	ATOMIC WEIGHT*
silver	Ag	107.880	lead	Pb	207.21
arsenic	As	74.91	rubidium	Rb	85.48
gold	Au	197.2	antimony	Sb	121.76
bismuth	Bi	209.00	selenium	Se	78.96
germanium	Ge	72.60	tin	Sn	118.70
potassium	K	39.096	tellurium	Te	127.61
sodium	Na	22.997	thallium	Tl	204.39

* As published in the Journal of the American Chemical Society, April 1950.

A.2 Interconversion of weight and atomic percentages in binary alloy systems

If w_x and a_x represent the weight and atomic percentages of one component having atomic weight x, and if w_y, a_y and y represent the corresponding quantities for the second component, then:

$$w_y = 100 - w_x$$
$$a_y = 100 - a_x$$

The conversion from weight to atomic percentages, or vice versa, may be made by use of the following formulae:

$$a_x = \frac{100}{1 + (x/y)[(100/w_x) - 1]}$$

$$w_x = \frac{100}{1 + (y/x)[(100/a_x) - 1]}$$

A.3 Phase diagrams (courtesy of ASM International)

A.3.1 Alloying elements with zero or very low primary solid solubilities

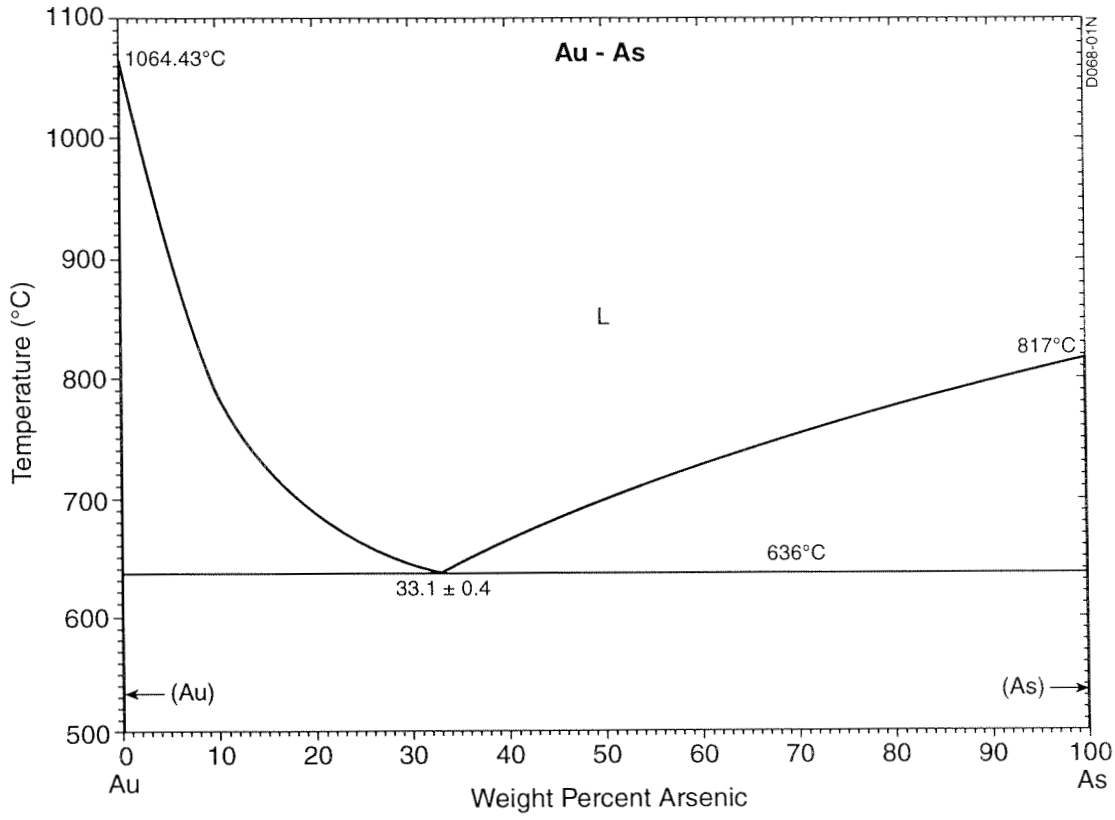

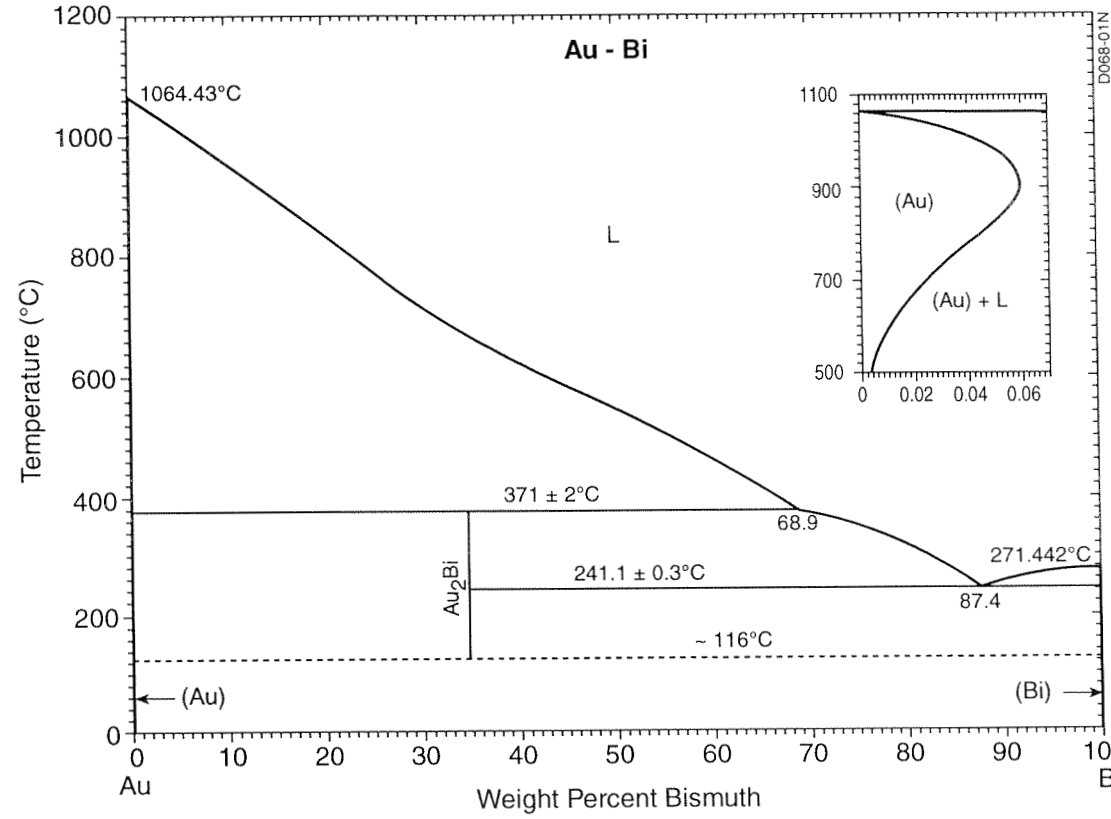

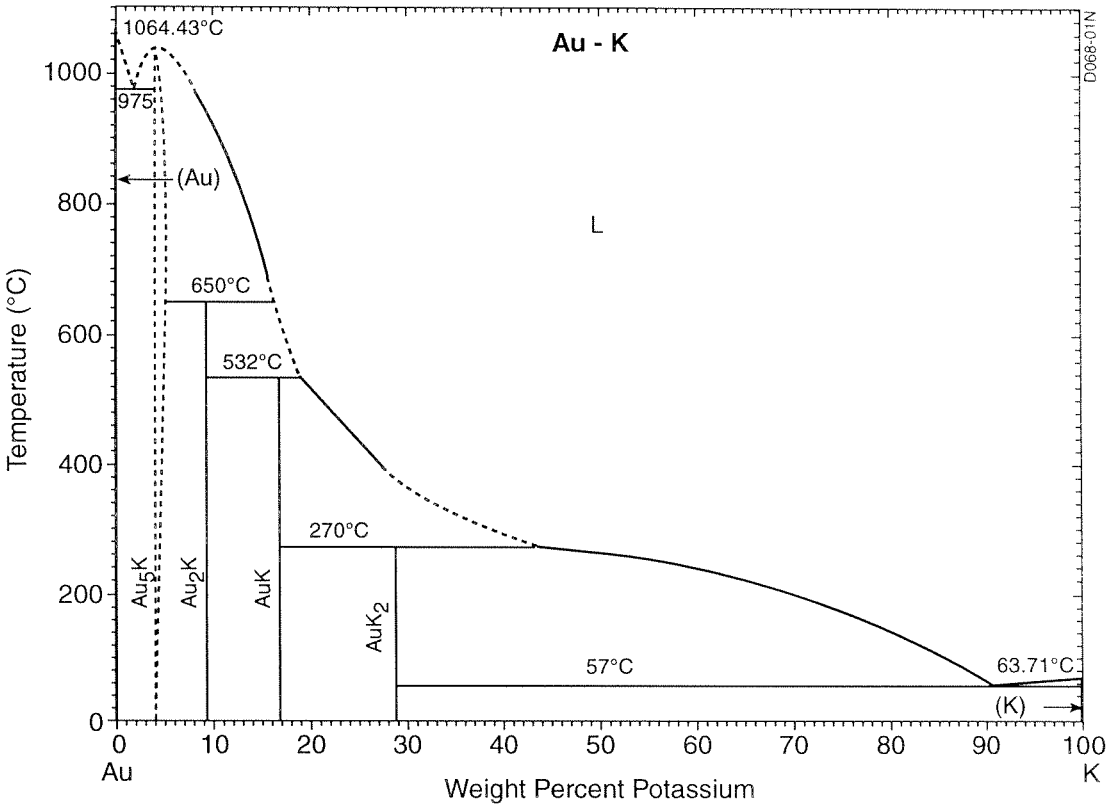
Au - K
1064.43°C
975
(Au)
L
650°C
532°C
270°C
57°C
63.71°C
(K)
Au5K
Au2K
AuK
AuK2
Temperature (°C)
Weight Percent Potassium
Au
K
D068-01N

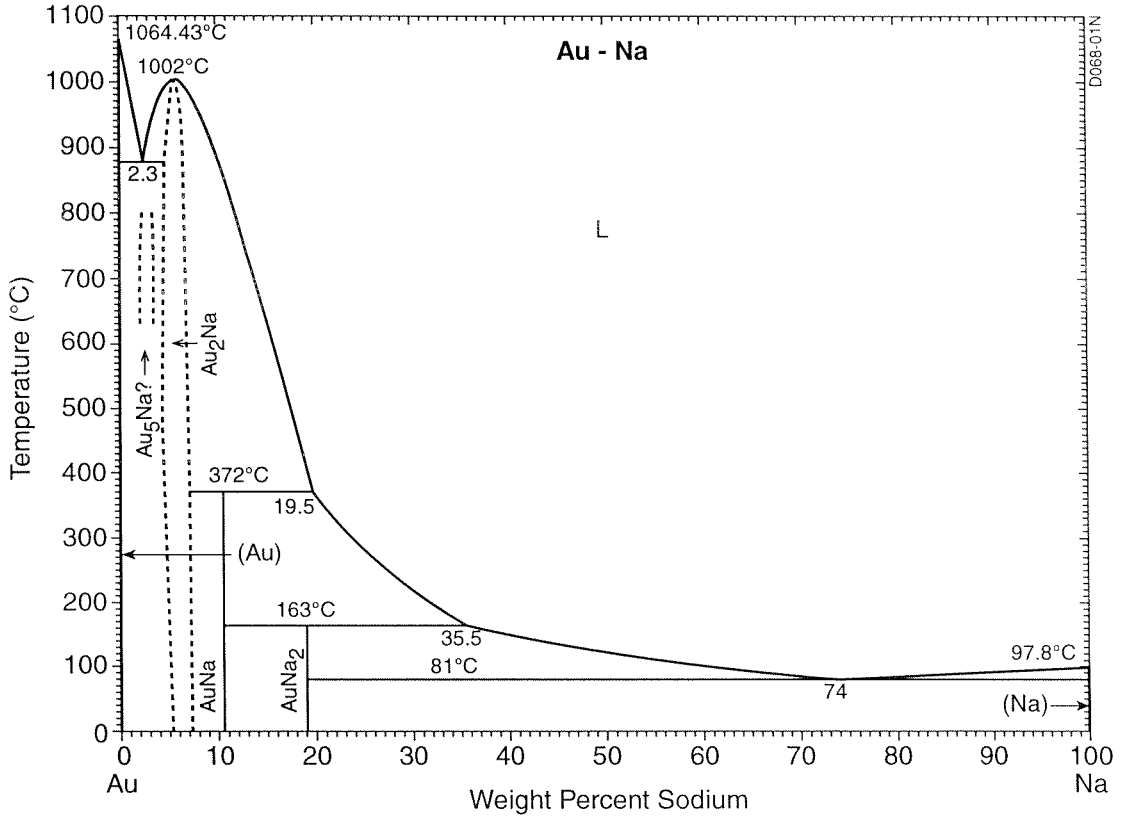
Au - Na
1064.43°C
1002°C
2.3
L
Au5Na?
Au2Na
372°C
19.5
(Au)
163°C
35.5
81°C
74
97.8°C
(Na)
AuNa
AuNa2
Temperature (°C)
Weight Percent Sodium
Au
Na
D068-01N

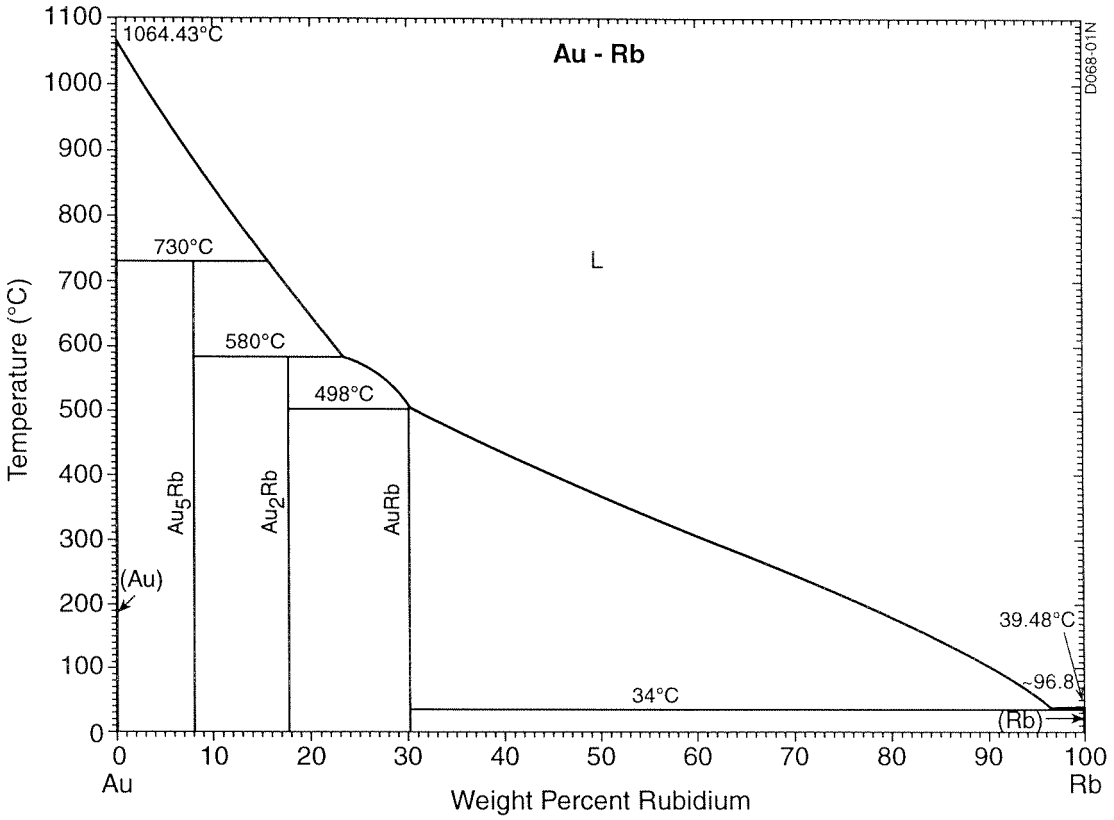
Au - Rb
D068-01N
1064.43°C
730°C
580°C
498°C
L
Au_5Rb
Au_2Rb
AuRb
(Au)
39.48°C
~96.8
34°C
(Rb)
Temperature (°C)
Weight Percent Rubidium
Au
Rb

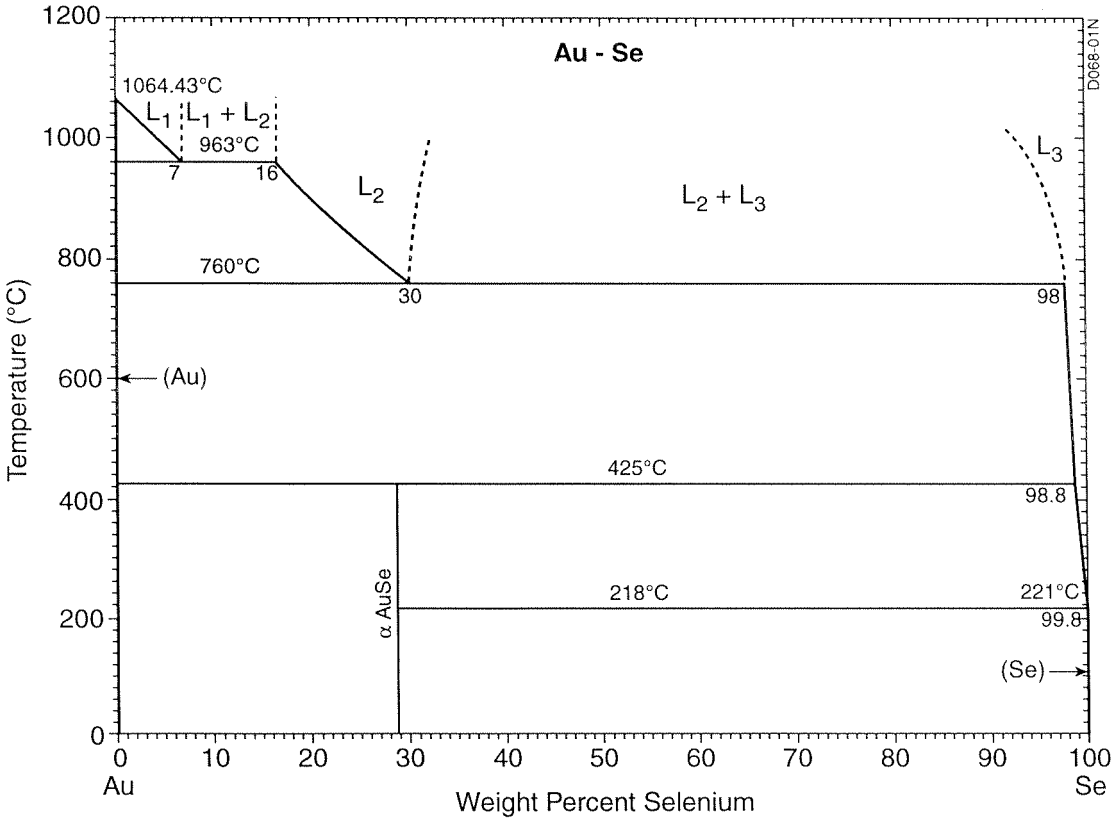
Au - Se
D068-01N
1064.43°C
L_1
$L_1 + L_2$
963°C
7
16
L_2
$L_2 + L_3$
L_3
760°C
30
98
(Au)
425°C
98.8
α AuSe
218°C
221°C
99.8
(Se)
Temperature (°C)
Weight Percent Selenium
Au
Se

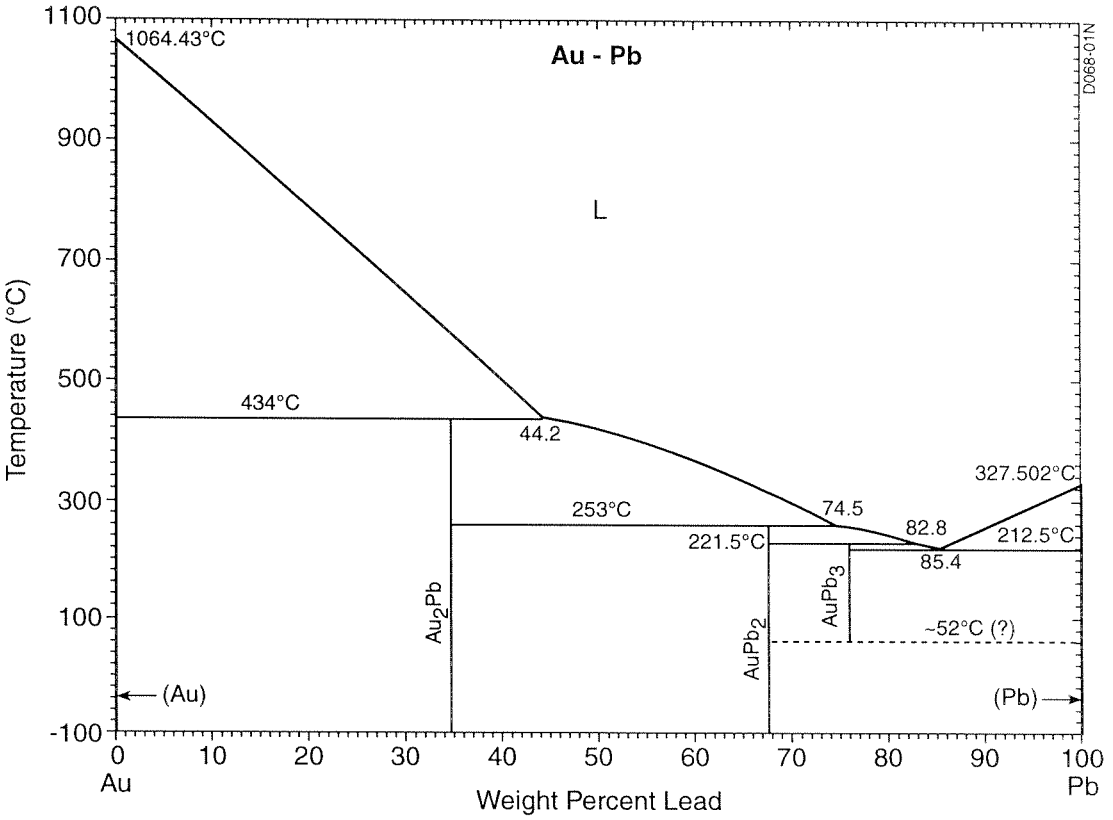
Au - Pb
D068-01N
1064.43°C
L
434°C
44.2
327.502°C
253°C
74.5
82.8
212.5°C
221.5°C
85.4
Au_2Pb
$AuPb_3$
$AuPb_2$
~52°C (?)
(Au)
(Pb)
Temperature (°C)
1100
900
700
500
300
100
-100
0
10
20
30
40
50
60
70
80
90
100
Au
Pb
Weight Percent Lead

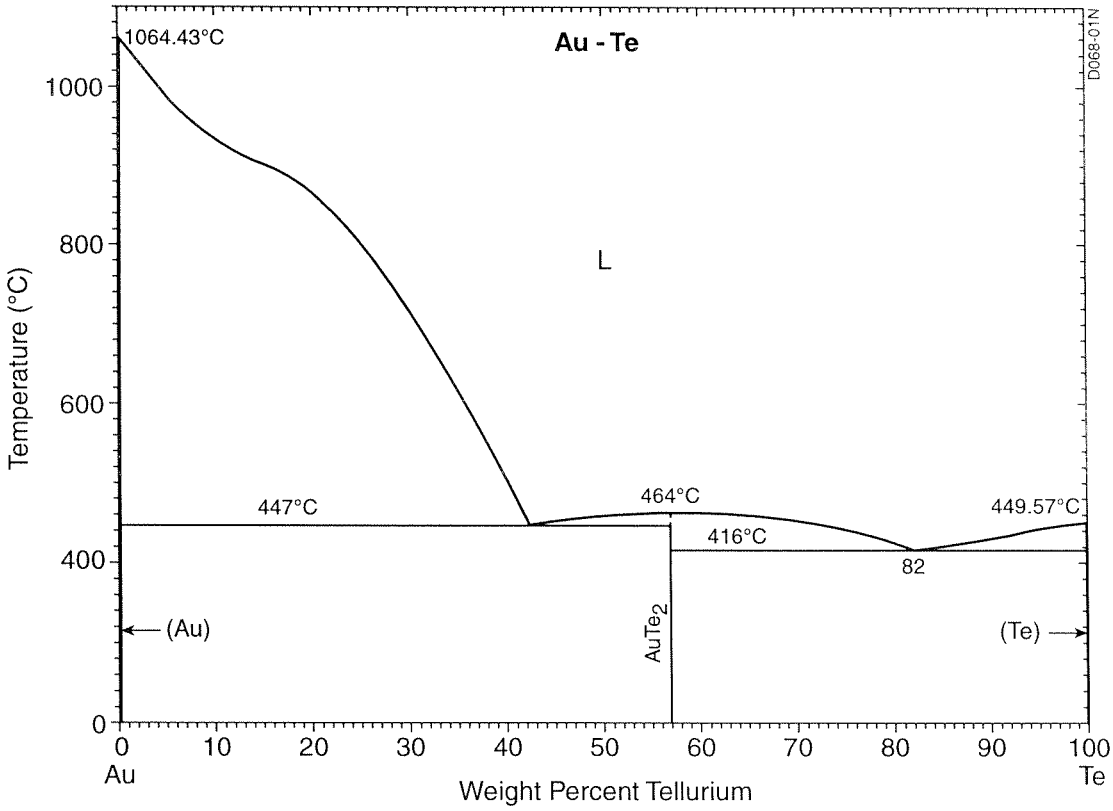
Au - Te
D068-01N
1064.43°C
L
447°C
464°C
449.57°C
416°C
82
$AuTe_2$
(Au)
(Te)
Temperature (°C)
1000
800
600
400
0
0
10
20
30
40
50
60
70
80
90
100
Au
Te
Weight Percent Tellurium

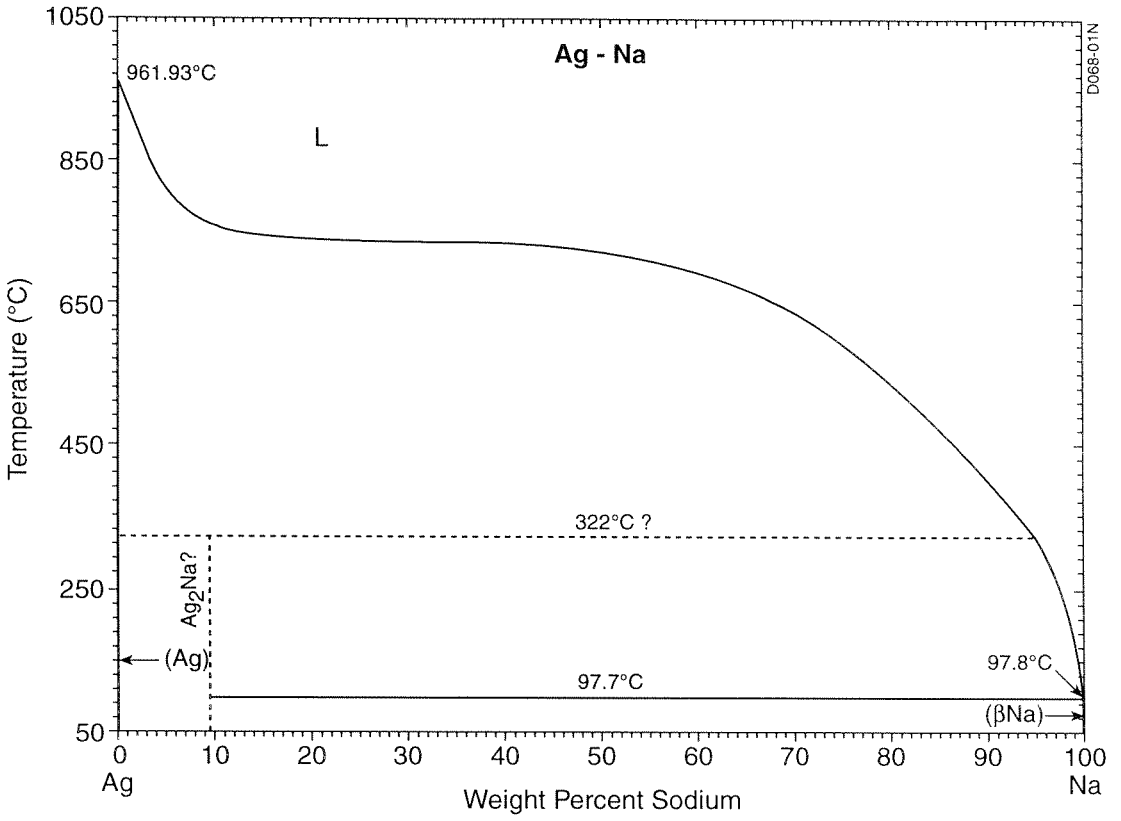
Ag - Na
961.93°C
L
322°C ?
Ag2Na?
(Ag)
97.7°C
97.8°C
(βNa)
Temperature (°C)
Weight Percent Sodium
Ag
Na
D068-01N

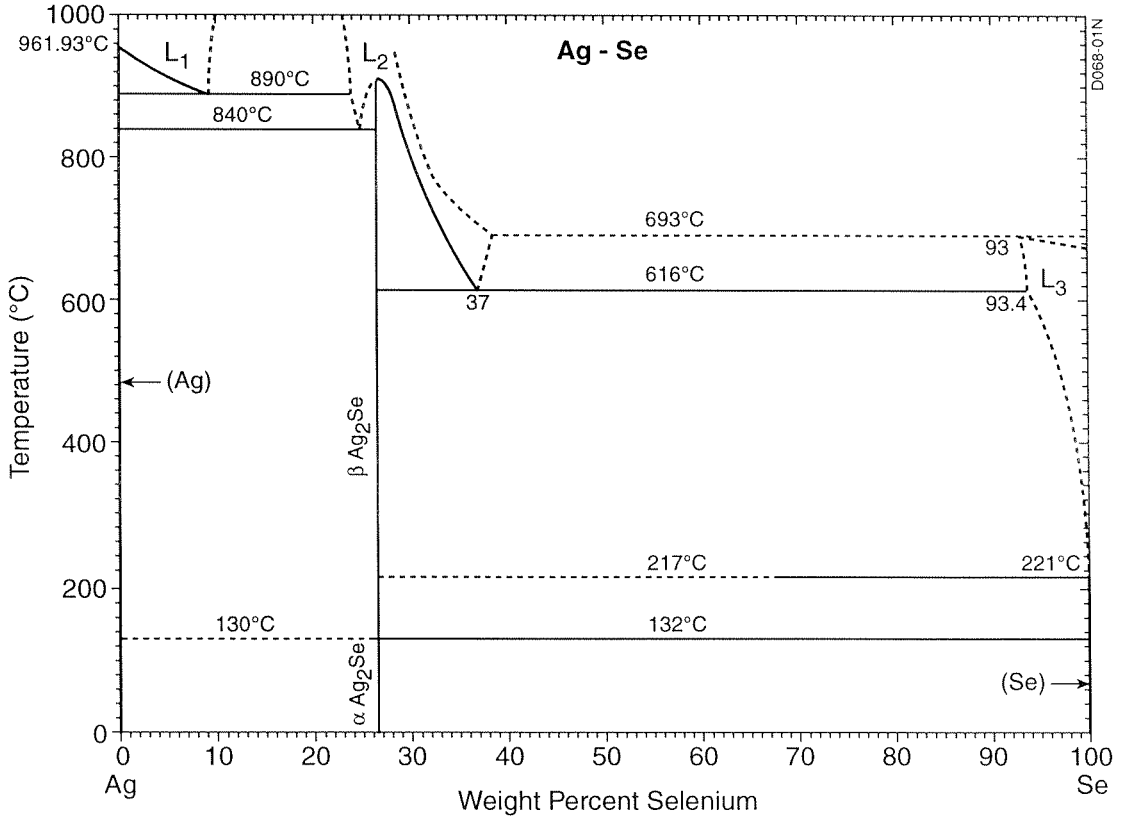
Ag - Se
961.93°C
L1
890°C
840°C
L2
693°C
93
616°C
37
93.4
L3
(Ag)
β Ag2Se
217°C
221°C
130°C
132°C
α Ag2Se
(Se)
Temperature (°C)
Weight Percent Selenium
Ag
Se
D068-01N

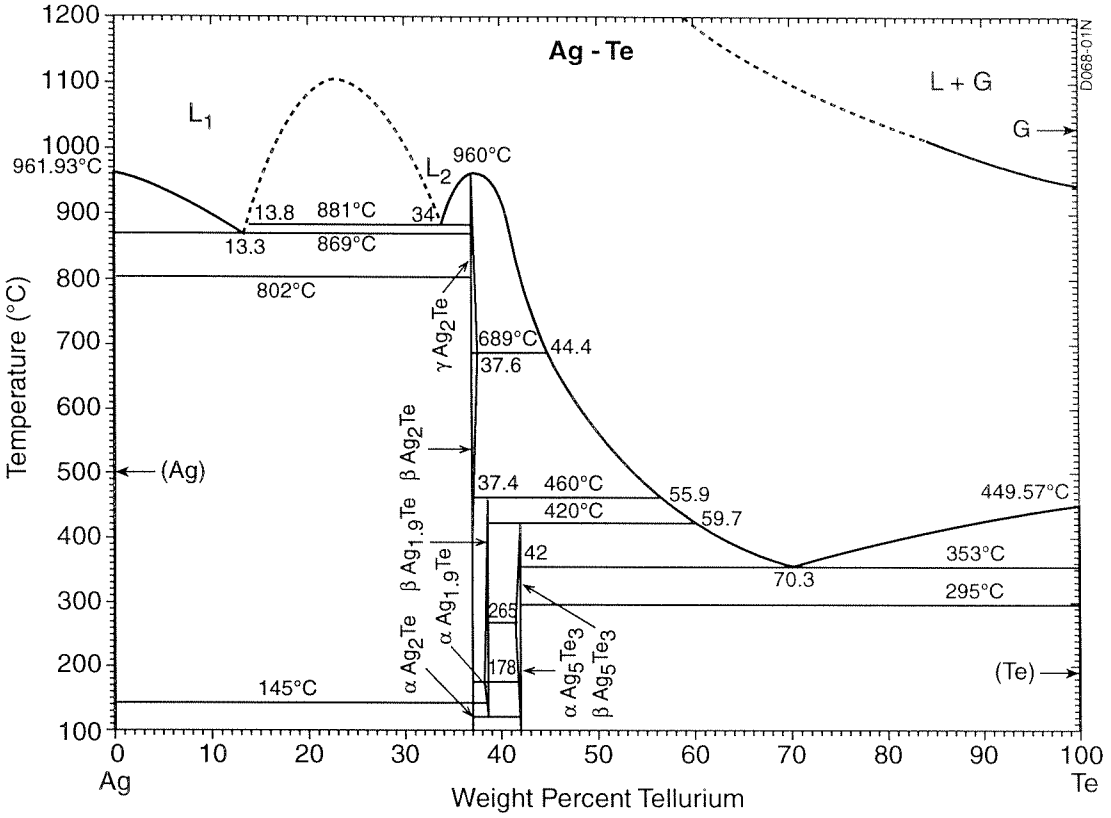
Ag - Te
L + G
G
L1
L2
960°C
961.93°C
13.8
881°C
34
13.3
869°C
802°C
γ Ag2Te
689°C
44.4
37.6
β Ag2Te
37.4
460°C
55.9
449.57°C
420°C
59.7
β Ag1.9Te
42
353°C
70.3
295°C
265
α Ag1.9Te
α Ag2Te
178
α Ag5Te3
β Ag5Te3
145°C
(Ag)
(Te)
Temperature (°C)
Weight Percent Tellurium
Ag
Te
D068-01N

A.3.2 Alloying elements with maximum primary solid solubilities at eutectic or peritectic temperatures

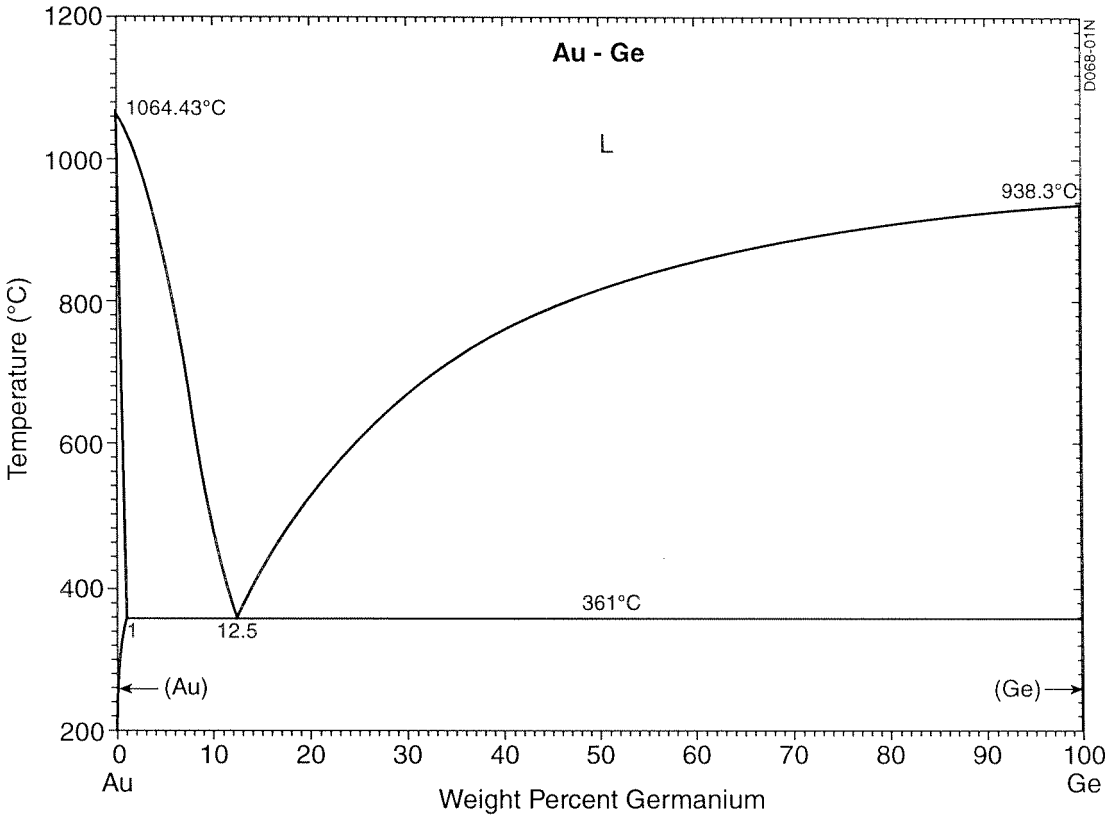

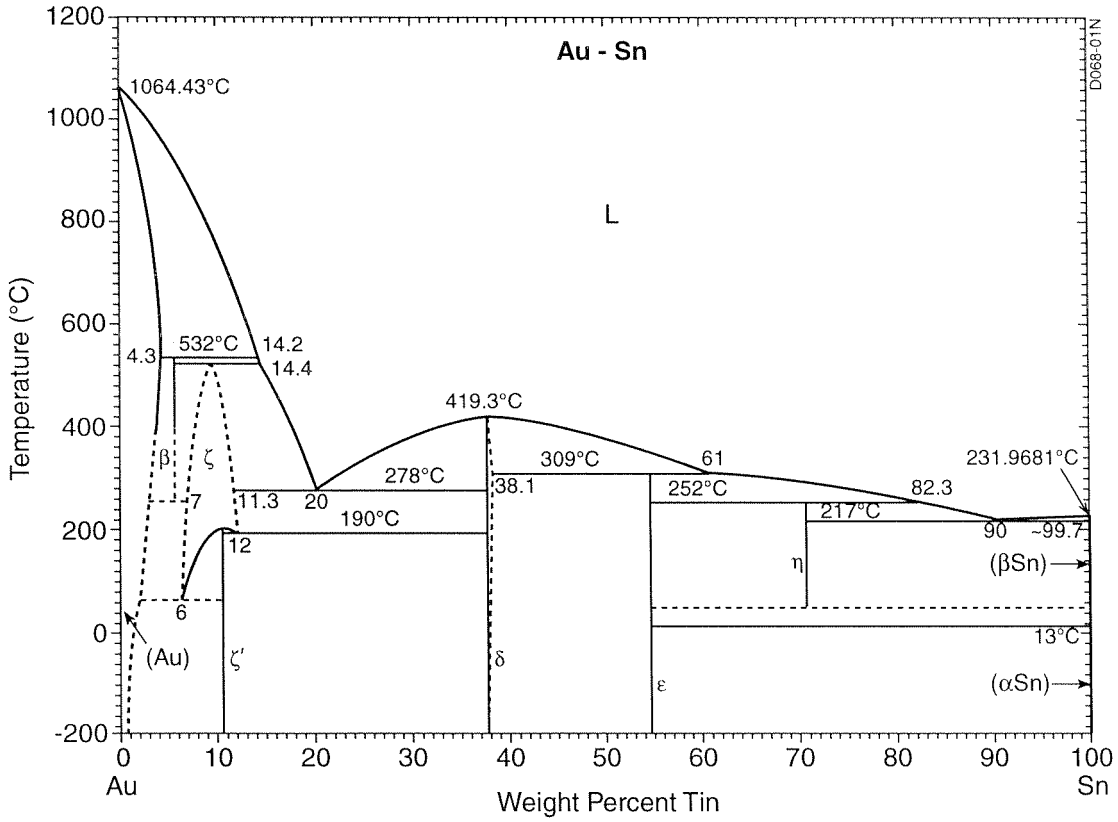

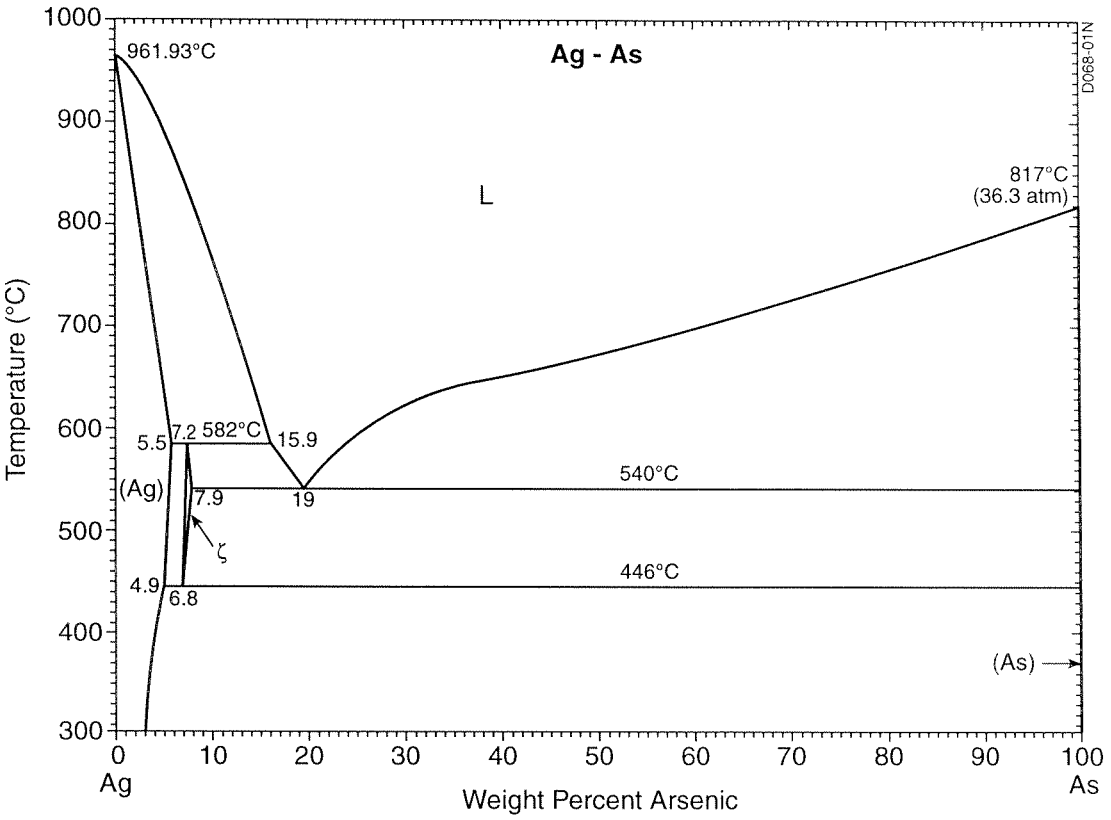
Ag - As
961.93°C
817°C
(36.3 atm)
L
5.5
7.2
582°C
15.9
540°C
(Ag)
7.9
19
ζ
4.9
6.8
446°C
(As)
Temperature (°C)
1000
900
800
700
600
500
400
300
0
10
20
30
40
50
60
70
80
90
100
Ag
As
Weight Percent Arsenic
D068-01N

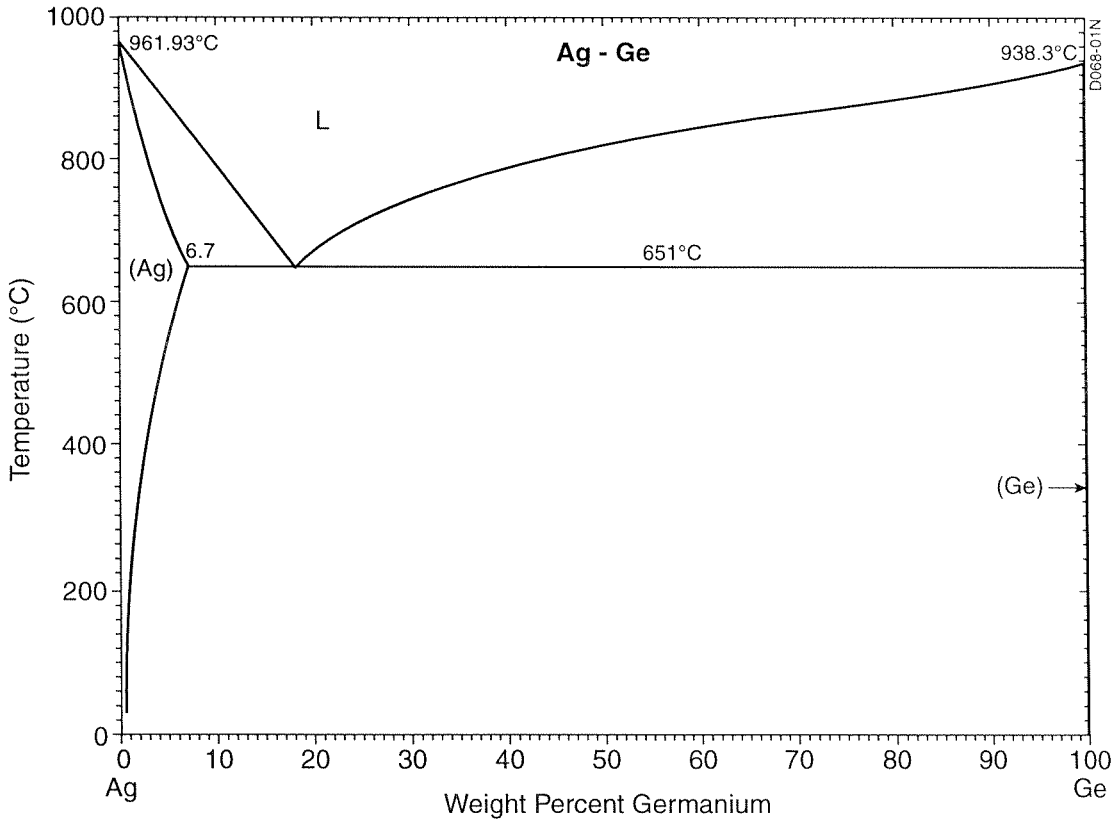
Ag - Ge
961.93°C
938.3°C
L
6.7
(Ag)
651°C
(Ge)
Temperature (°C)
1000
800
600
400
200
0
0
10
20
30
40
50
60
70
80
90
100
Ag
Ge
Weight Percent Germanium
D068-01N

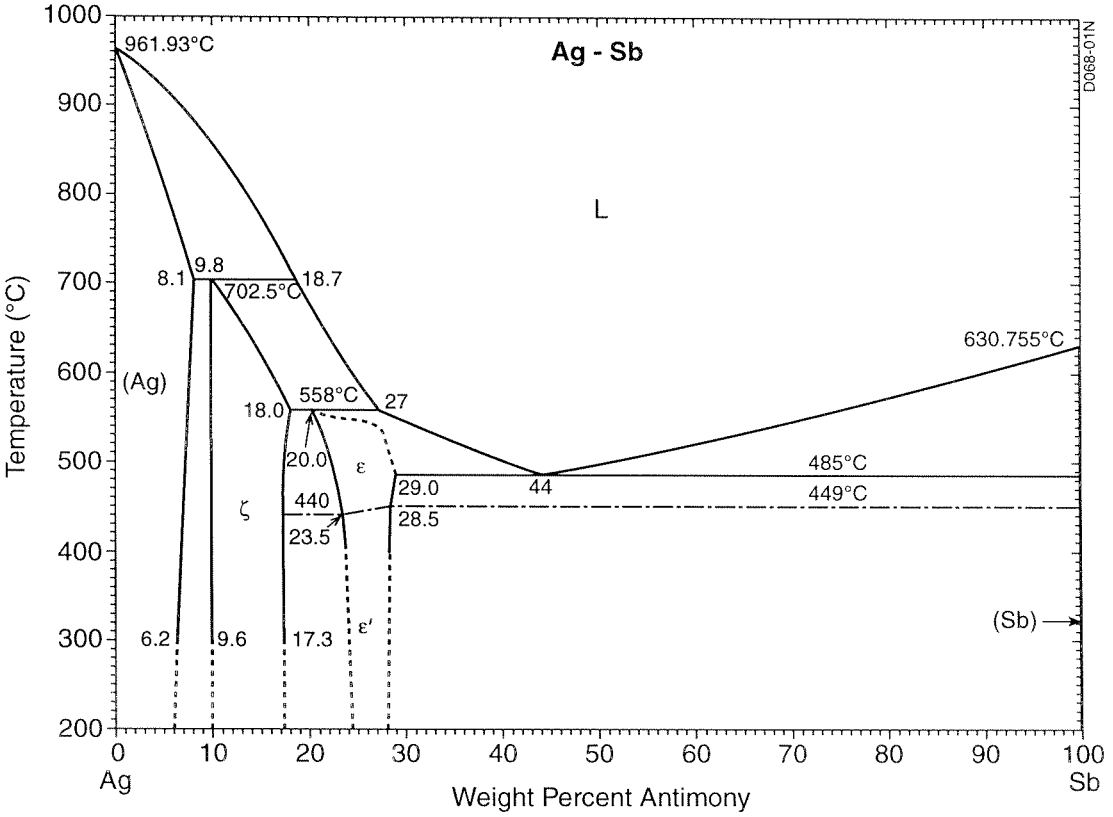
Ag - Sb
D068-01N
961.93°C
L
8.1
9.8
18.7
702.5°C
630.755°C
(Ag)
18.0
558°C
27
20.0
ε
485°C
29.0
44
449°C
440
ζ
23.5
28.5
6.2
9.6
17.3
ε'
(Sb)
Temperature (°C)
1000
900
800
700
600
500
400
300
200
0
10
20
30
40
50
60
70
80
90
100
Ag
Sb
Weight Percent Antimony

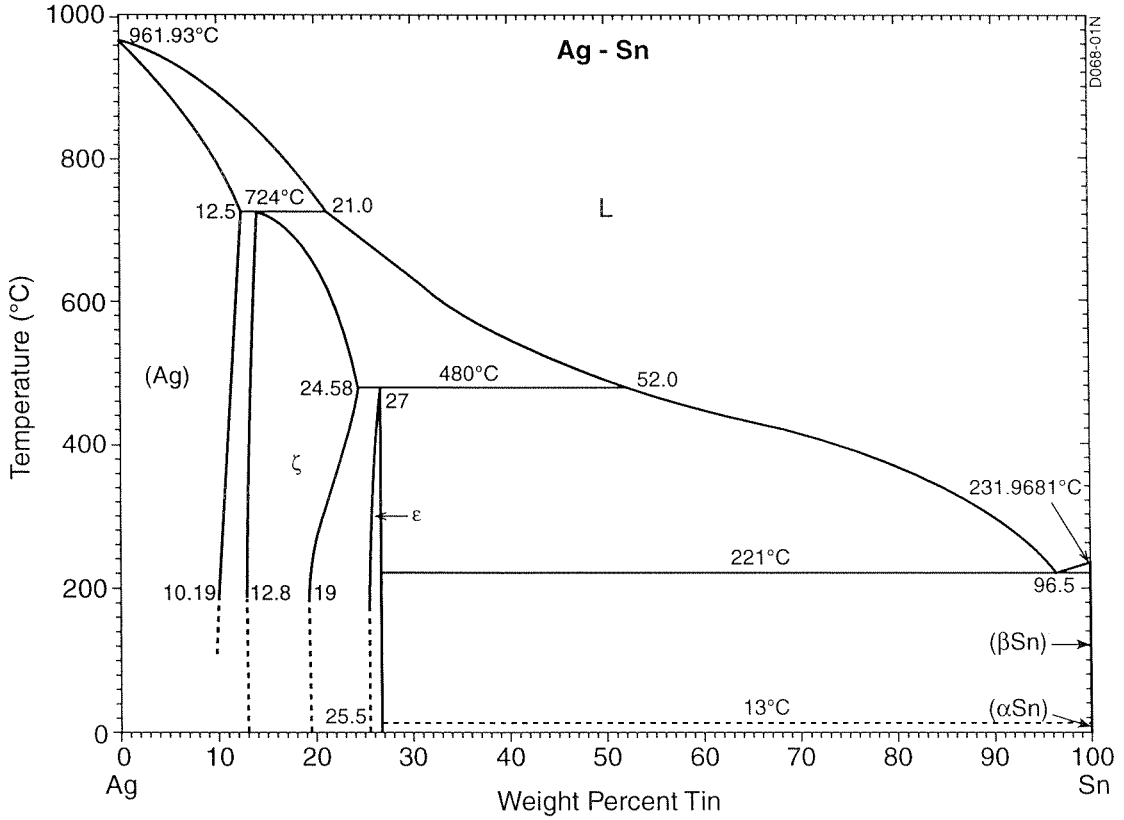
Ag - Sn
D068-01N
961.93°C
L
12.5
724°C
21.0
(Ag)
24.58
480°C
52.0
27
ζ
ε
231.9681°C
221°C
96.5
10.19
12.8
19
(βSn)
25.5
13°C
(αSn)
Temperature (°C)
1000
800
600
400
200
0
0
10
20
30
40
50
60
70
80
90
100
Ag
Sn
Weight Percent Tin

A.3.3 Alloying elements with maximum primary solid solubilities above eutectic temperatures

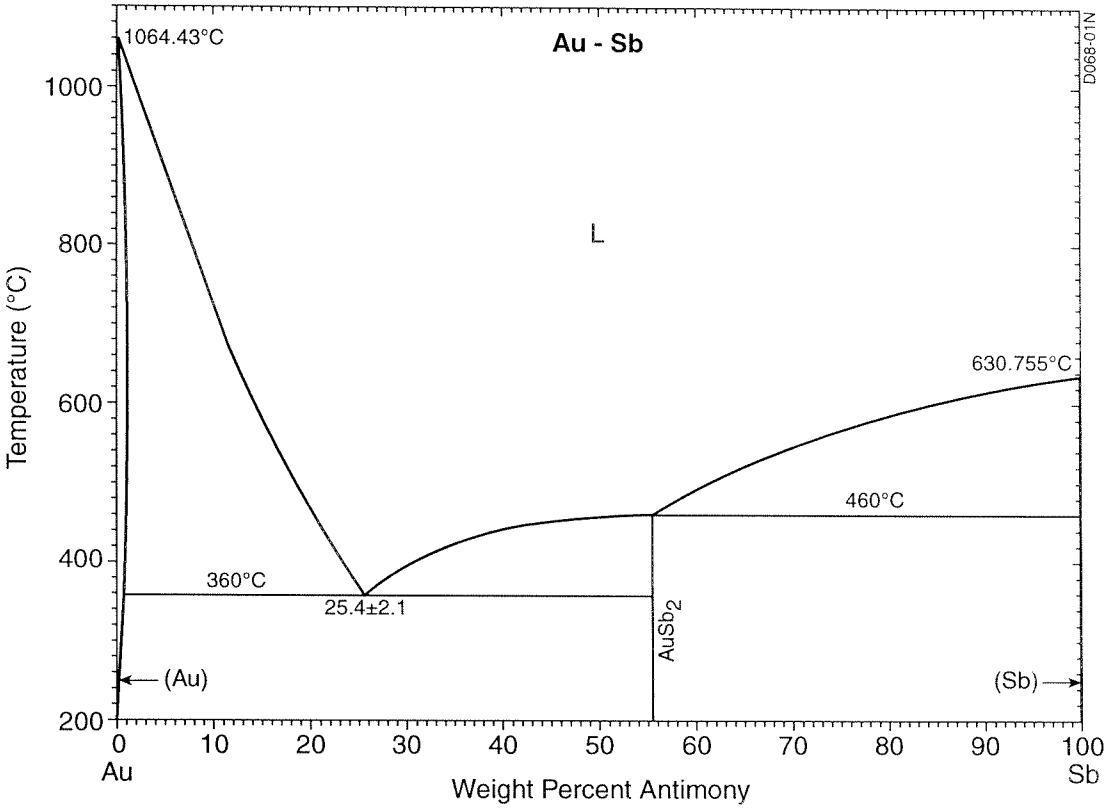

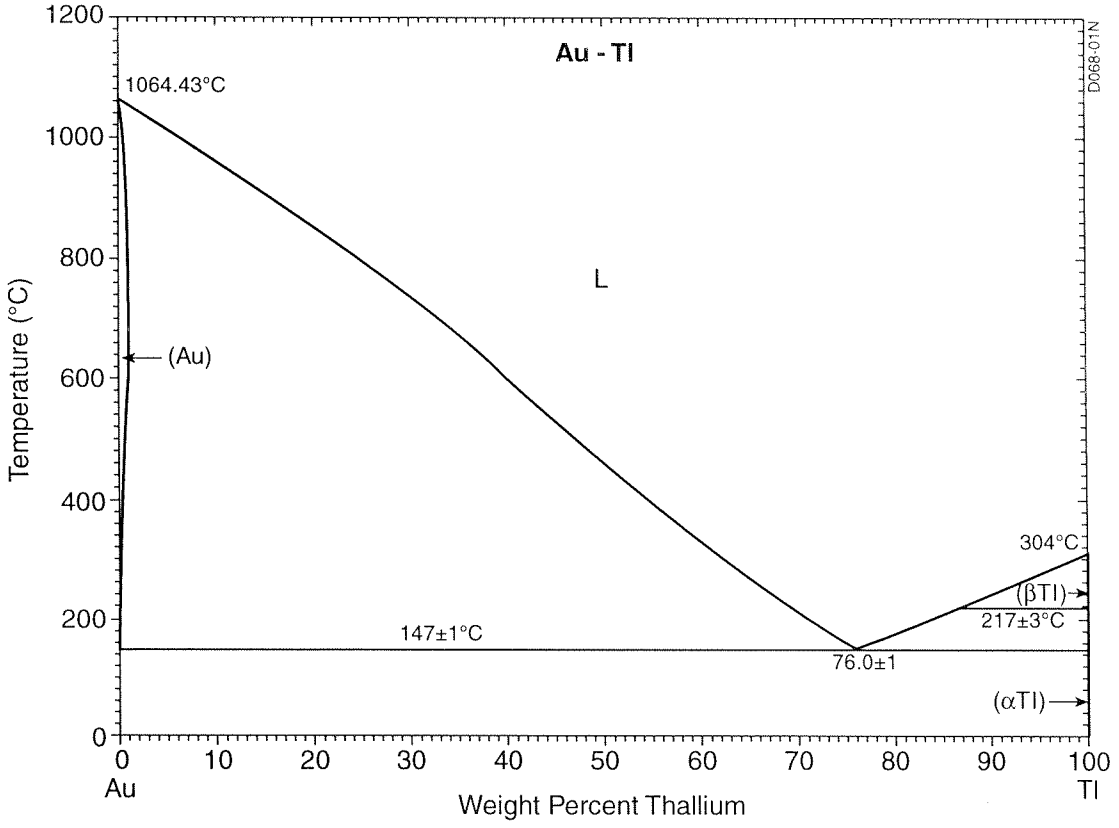

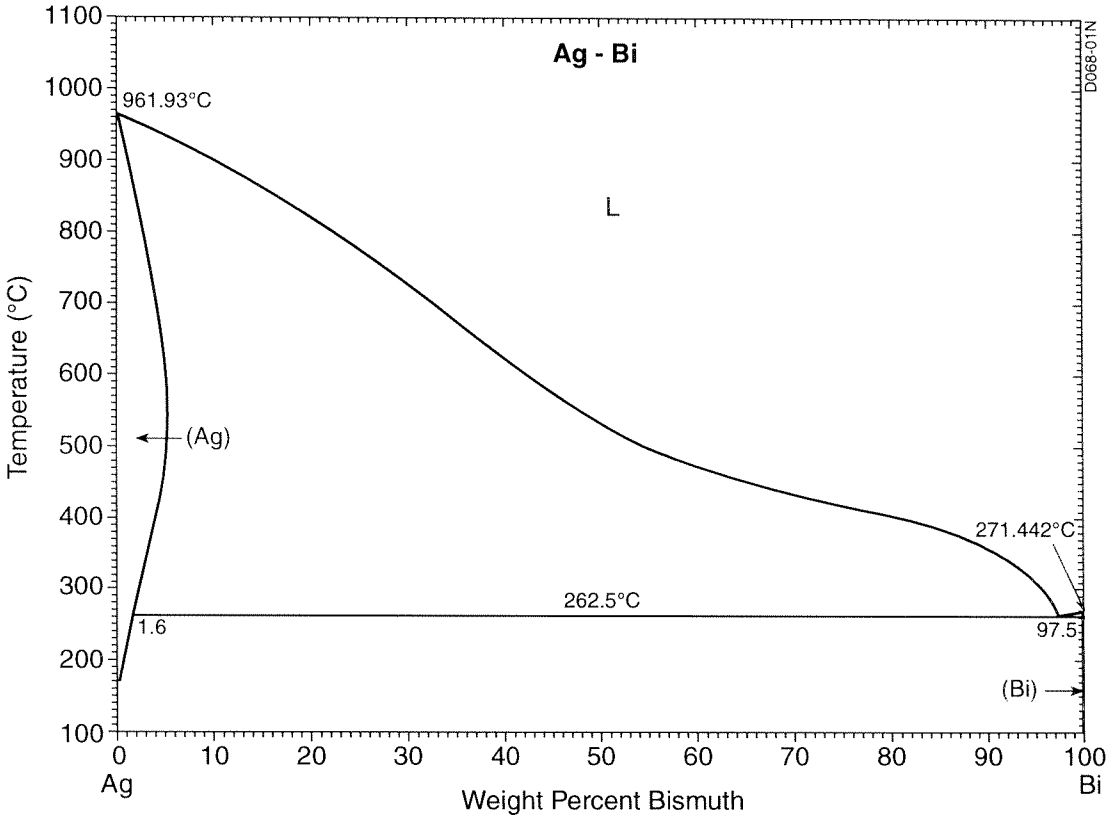
Ag - Bi
D068-01N
961.93°C
L
(Ag)
271.442°C
262.5°C
1.6
97.5
(Bi)
Temperature (°C)
1100
1000
900
800
700
600
500
400
300
200
100
0
10
20
30
40
50
60
70
80
90
100
Ag
Bi
Weight Percent Bismuth

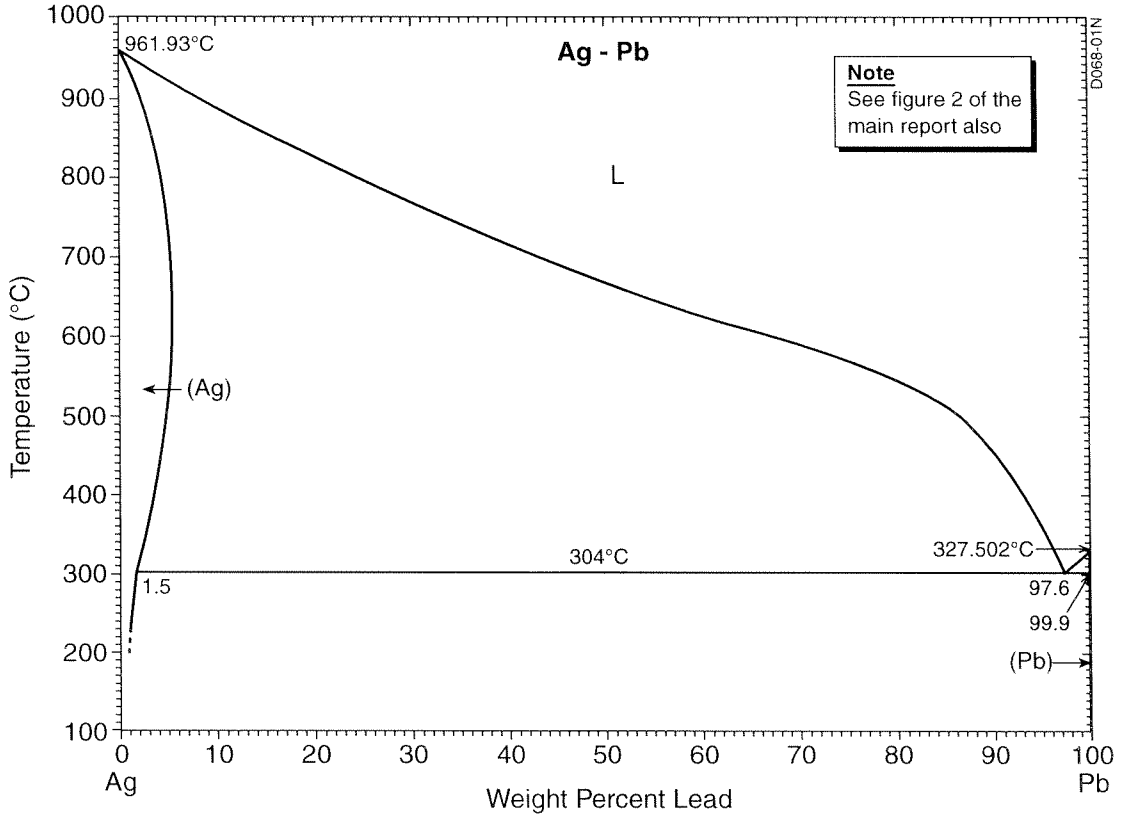
Ag - Pb
D068-01N
961.93°C
Note
See figure 2 of the main report also
L
(Ag)
304°C
327.502°C
1.5
97.6
99.9
(Pb)
Temperature (°C)
1000
900
800
700
600
500
400
300
200
100
0
10
20
30
40
50
60
70
80
90
100
Ag
Pb
Weight Percent Lead

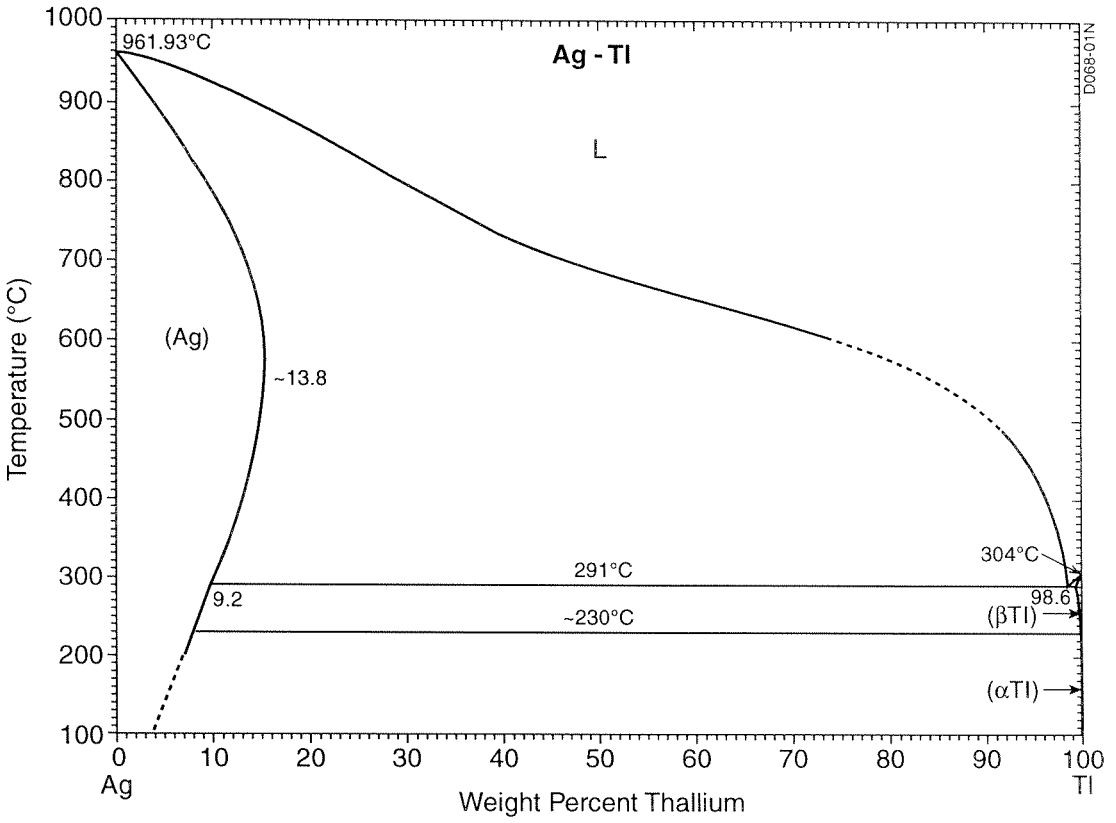
Ag - Tl
961.93°C
L
(Ag)
~13.8
9.2
291°C
304°C
98.6
~230°C
(βTl)
(αTl)
Temperature (°C)
1000
900
800
700
600
500
400
300
200
100
0
10
20
30
40
50
60
70
80
90
100
Ag
Tl
Weight Percent Thallium
D068-01N

Appendix B Classification of archaeological silver artifacts and coins in support of figure 11

B.1 Table B.1: artifacts

Table B.1 Classification and weight % of actually and potentially embrittling impurity elements in archaeological silver artifacts

85 ≤ Ag wt.% < 95							95 ≤ Ag wt.%						REFERENCES AND COMMENTS
Pb	Bi	Sb	Sn	Pb	Bi	Sb	Sn	Pb	Bi	Sb	Sn		
0.2								0.2				0.3	
0.5								0.4					Lucas (1928)
0.2	0.19			0.2				0.5				0.1	
0.2	0.18			0.5				0.2				0.5	Gale and Stos-Gale (1981a)
1.6				0.4				0.5	0.19				One outlier (2.9 wt.% Pb; 1.5 wt.% Bi)
0.2	0.19			0.2				0.2	0.19				excluded
0.2				0.71				0.1					
1.68	<0.01	<0.10	^					0.42	0.19	<0.10	^	0.30	<0.01	<0.10	^		
1.65	<0.01	0.10	|					0.39	0.15	0.20	|	0.25	<0.01	0.18	|		
1.10	<0.01	0.08	|					0.56	<0.01	<0.10	|	0.06	0.15	<0.10	|		
1.15	0.18	0.33	|					0.50	<0.01	<0.10	|	0.45	0.10	<0.10	|		
0.71	0.22	0.21	|					0.43	0.06	<0.10	|	0.46	<0.01	0.11	|		
0.90	0.04	0.21	|					0.44	0.05	0.14	|	0.43	<0.01	0.35	|		Bennett (1994)
0.73	0.05	0.22	<0.1					0.45	<0.01	0.15	|	2.70	0.15	<0.10	<0.1		
0.81	0.07	0.21	|					0.41	<0.01	0.18	<0.1	0.84	<0.01	0.40	|		All analyses: less than 0.1 wt.% Sn
1.18	0.06	0.17	|					0.22	0.21	0.10	|	0.53	0.04	<0.10	|		and less than 0.005 wt.% As
0.53	0.04	0.15	|					0.97	<0.01	0.15	|	1.17	0.05	0.44	|		
1.05	0.08	0.23	|					0.18	0.16	0.15	|	1.08	0.07	0.20	|		
1.04	0.03	0.50	|					0.16	0.17	0.13	|	0.46	0.03	<0.10	|		
0.91	0.07	0.21	>					0.16	0.26	0.18	|	0.44	0.02	0.14	|		
								0.25	<0.01	<0.1	|	0.22	<0.01	0.23	>		
								0.46	0.07	<0.10	>						

85 ≤ Ag wt.% < 95														
Pb	Sn	Pb	Sn	Pb	Sn	Pb	Sn	Pb	Sn	Pb	Sn			
0.8	0.385	0.3		0.6	0.129	2.0		0.8	0.003	1.2	0.051	0.7		
0.3	0.022	1.0	0.043	1.2	0.013	1.0		1.5	0.185	0.7		0.9		
0.4	0.063	0.5	0.024	1.7		1.0		0.2	0.012	1.3		0.014	0.1	
0.7		0.8		0.8		0.6	0.073	0.4		1.7			0.2	
0.6		0.4		0.7	0.19	1.4	0.018	0.3	0.233			0.014	0.3	Perea and Rovira (1995)
1.3		0.4		0.6	0.092	0.4	0.267	0.4				0.005	0.2	
0.5		0.2	0.024	1.7		0.2		0.4	0.016			0.007	0.2	One analysis for 85 ≤ Ag wt.% < 95 gave
0.6	0.228	0.2		3.4		1.0	0.018	0.5	0.035			0.005	0.2	0.15 wt.% Sb
0.6	0.340	1.9	0.052	2.4		0.2	0.006	0.3	0.032			0.036	0.7	

Table B.2 Classification and weight % of actually and potentially embrittling impurity elements in archaeological silver coins

85 ≤ Ag wt.% < 95								95 ≤ Ag wt.%								REFERENCES AND COMMENTS
Pb	Sn	Pb	Sn	Pb	Sn	Pb	Sn	Pb	Sn	Pb	Sn	Pb	Sn	Pb	Sn	
0.57	0.17	0.88		0.85	0.08	0.23	0.02	0.46		2.19		0.72	0.06	3.68		
1.09	0.02	0.47		0.63	0.08	0.25	0.04	0.63		0.85		2.87		0.13		Caley (1964)
1.22	0.04	0.37	0.26	0.39	0.17			1.03		0.86		3.05		0.43		
0.39	0.23															Tylecote (1992)
0.38		1.05		0.44				0.25								
0.37		0.78		1.02												Cope (1972)
0.95		0.34		0.61												
0.5		0.2						0.3		0.2		0.6				
0.6		4.7						0.7		0.7						MacDowall (1972)
1.58	0.05	1.48	0.10	1.10	0.05			0.68	0.07	1.10	0.01					
1.85	0.12	1.63	0.10					0.42	0.10							Gordus (1972)
	0.4		0.1		0.8	0.2										
	0.9		0.5		0.3	0.3										
	1.4		0.7		0.6											Metcalf (1972)
	0.5		0.8		0.1											

85 ≤ Ag wt.% < 95															95 ≤ Ag wt.%			
Pb	Bi	Sn	Pb	Bi	Sn	Pb	Bi	Sn	Pb	Bi	Sn	Pb	Bi	Sn	Pb	Bi	Sn	
1.5	0.0	2.9	1.0	0.0		1.2	0.0	0.5	1.3	0.1	0.8	1.7	0.0	0.0	0.1		0.0	
2.4	0.2	1.7	2.8	0.2	0.5	1.4	0.1	0.2	1.1	0.2	0.9	1.1	0.0		0.7		0.0	
2.5	0.0	0.2	1.1	0.0	0.0	0.9	0.1	0.6	1.3	0.0	0.0	1.4	0.1		1.0	0.1		
2.0	0.0	0.0	0.6	0.2	0.5	1.1	0.2	0.2	1.2	0.2	0.3	1.6	0.2	0.4	1.0			
1.1	0.1	0.1	0.8	0.1	0.2	1.4	0.0		1.6	0.1	0.7	1.4	0.3	0.2	0.5	1.3	0.0	
1.7	0.1	0.2	1.4	0.2	0.3	1.3	0.2	0.3	1.6	0.0		1.7	0.0		0.6	0.3	0.0	
0.9	0.0	0.1	0.9	0.2		1.2	0.0	0.2	1.2	0.1		1.2	0.3		0.6	0.4	0.0	McKerrell and Stevenson (1972)
1.4	0.1	0.3	1.6	0.1		0.9	0.0	0.2	1.9	0.0		1.4	0.2	0.3	0.9	0.2	0.0	
0.7	0.0	0.3	1.3	0.0	0.2	1.4	0.3	0.5	0.8	0.1	0.3	1.3	0.1	0.1	0.6	0.2	0.0	One outlier (0.6 wt.% Pb; 8.7 wt.% Bi;
1.3	0.2	0.5	0.8	0.0		1.2	0.1	0.3	1.4	0.2	0.6	1.3	0.0		0.4	1.0	0.0	0 wt.% Sn) excluded
0.9	0.1	0.6	1.3	0.0	0.1	1.2	0.2	0.6	1.3	0.2	0.0	1.9	0.0		0.3	0.7	0.0	
1.2	0.2	0.3	1.2	0.1	1.0	1.0	0.0	0.4	1.4	0.0		1.1	0.0		0.9	0.2	0.0	
0.7	0.0	0.1	1.2	0.0	0.4	1.3	0.3	0.9	1.8	0.1	0.5	0.9	0.0		0.3	1.3	0.0	
1.0	0.1	0.3	1.9	0.3	0.2	1.3	0.2	0.3	1.4	0.2	0.2	1.2	0.2	0.0	0.2	0.5	0.0	
0.8	0.0	0.0	0.9	0.1	0.3	0.9	0.1		1.4	0.1	0.1	1.0	0.0	0.2				
1.4	0.1	0.3	1.4	0.2	0.6	1.6	0.2		2.0	0.2	0.5	1.0	1.2	0.0				
1.0	0.0	0.0	0.6	0.1	0.2	2.6	0.2	0.3	1.3	0.0	0.0	0.9	1.3	0.0				
0.9	0.1	0.3	1.0	0.1	0.4	2.5	0.1		1.4	0.2		0.7	0.8	0.2				
1.1	0.0		1.1	0.2	0.5	1.5	0.0		1.3	0.0								

Appendix C Classification of damaged archaeological gold artifacts in support of figure 12

C.1 Table C.1: Artifacts illustrated in Hartmann (1970, 1982)

Table C.1 Sample numbers, compositions and fracture classifications of archaeological gold artifacts illustrated in Hartmann (1970, 1982) and showing possible or probable evidence of low ductility or brittle fracture. The fracture classification codes are as follows:

* : intersecting or branching tears or cracks
AAMP : acute angled missing pieces
ALDT/C : *apparently* low ductility tears or cracks
LDT/C : low ductility tears or cracks
LDC : low ductility cracks

See Appendix C.2 for the criteria pertaining to the fracture classifications and codes.

SAMPLE NUMBER	ALLOY AND IMPURITY ELEMENTS (wt.%)				FRACTURE CLASSIFICATIONS			FRACTURE CLASSIFICATION CODES				
	Ag	Cu	Sn	Pb, Bi, Sb	*PROBABLY* BRITTLE	*POSSIBLY* BRITTLE I	*POSSIBLY* BRITTLE II	*	AAMP	ALDT/C	LDT/C	LDC
1	16	4.75	0.10			•		o	o			
5	11.5	0.31	0.02				•		o			
6	12.5	0.27	0.01				•		o			
12	10	0.32	<0.01				•		o	o		
16	21	1.05	0.03				•		o			
101	23	1.58	0.20				•		o			
113	14	0.89	0.02				•		o			
149	14.5	0.03					•					o
193	20	1.57	0.09				•		o			
195	18.5	1.67	0.13				•		o			
239	10	6.10	0.10				•		o	o		
254	27	1.29	0.26				•		o	o		
300	23	2.10	0.02				•			o		
312	17	0.90	0.09				•					o
313	19.5	1.58	0.04				•			o		
322	29	0.48	0.02				•	o	o			
341	12	12.1	0.17			•			o		o	
346	12	1.97	0.09	0.24 Pb		•		o	o		o	
350	9	5.40	0.05	trace Pb			•			o		
354	9	0.67	0.01				•		o	o		
355	5	0.49	0.02				•		o	o		
391	7	3.47	0.45	0.03 Pb			•		o	o		
445	18	2.84	0.21	trace Bi			•		o			
446	21.5	2.14	0.06				•		o			
450	12	0.34	0.19			•			o		o	
458	21	0.78	0.03				•		o	o		
521	13.5	0.16	0.02				•		o			

CONTINUED ON NEXT PAGE

Table C.1 CONTINUED FROM PREVIOUS PAGE

SAMPLE NUMBER	ALLOY AND IMPURITY ELEMENTS (wt.%)				FRACTURE CLASSIFICATIONS			FRACTURE CLASSIFICATION CODES				
	Ag	Cu	Sn	Pb, Bi, Sb	*PROBABLY* BRITTLE	*POSSIBLY* BRITTLE I	*POSSIBLY* BRITTLE II	*	AAMP	ALDT/C	LDT/C	LDC
529	10	0.28	0.01			●		o		o		
545	17	0.30	0.02				●	o	o			
548	12	0.18	0.02			●		o	o			
555	12	0.36				●		o	o			
559	10	5.25	0.03			●		o	o			
575	12	4.82	0.07	0.025 Pb	●			o	o			
598	12	6.21	0.08				●			o		
618	23	3.53	0.04				●		o			
721	14	0.09	0.06			●		o	o			
724	15	0.12	0.03				●			o		
727	9	0.04	<0.01			●			o			o
729	11	0.08	<0.01			●		o	o			o
730	20	0.11	<0.01				●			o		
818	13	5.38	0.15	trace Pb			●					o
867	19	5.83	0.38				●					o
870	17	4.82	0.38				●					o
875	14	8.16	0.16				●			o		
925	16	3.83	0.48				●					o
926	13	3.81	0.38	trace Pb			●					o
929	12	6.29	0.04				●	o	o			
961	14	6.80	0.19				●			o		
976	19	5.93	0.01			●		o	o			
977	11	4.79	0.08			●		o	o			
979	11	5.96	0.23			●		o	o			
987	11	4.95	0.14				●			o		
1023	12	7.84	0.14				●	o	o	o		
1026	15.5	4.78	0.06				●		o	o		
1027	14.5	5.81	0.14				●		o	o		
1028	16	7.00	0.11			●		o	o			
1029	20	5.22	0.14			●		o	o	o		
1030	19	4.72	0.14			●		o	o	o		
1045	13	7.17	0.18			●			o	o		
1048	23	6.02	0.14				●		o	o		

CONTINUED ON NEXT PAGE

Table C.1

CONTINUED FROM PREVIOUS PAGE

SAMPLE NUMBER	ALLOY AND IMPURITY ELEMENTS (wt.%)				FRACTURE CLASSIFICATIONS			FRACTURE CLASSIFICATION CODES				
	Ag	Cu	Sn	Pb, Bi, Sb	*PROBABLY* BRITTLE	*POSSIBLY* BRITTLE I	*POSSIBLY* BRITTLE II	*	AAMP	ALDT/C	LDT/C	LDC
1059	11	4.87	0.17				●		o	o		
1061	19	1.98	0.01			●			o			o
1062	11	8.82		trace Pb			●		o			
1068	11	5.89	0.19				●			o		
1077	14	5.62	0.16				●		o	o		
1093	15	5.48	0.13				●		o			
1117	35	1.70	0.03	0.03 Pb; trace Bi		●		o	o			
1118	12	0.05	0.05				●			o		
1240	21	1.69	0.33				●		o			
1259	10	4.27	0.21	0.02 Sb			●	o	o			
1260	12	4.10	0.28	0.02 Sb			●	o	o			
1262	12	0.19	<0.01				●	o				
1295	18.5	0.50	0.03				●		o			
1303	10	0.14	0.03				●			o		
1306	14	1.68	0.18				●		o			
1332	11	0.52	0.08				●		o			
1334	15	1.67	0.03				●	o	o			
1392	21	2.37	0.21				●		o			
1491	27	3.01	0.08			●		o	o		o	
1492	27	3.27	0.10			●			o		o	
1493	27	2.87	0.11			●		o	o		o	
1494	26	4.51	0.12			●		o	o		o	
1645	12	1.56	0.04				●		o			
1646	13	2.53	0.13				●		o			
1647	17.5	2.79	0.11				●		o			
1648	19	2.05	0.13				●		o			
1707	6	0.22	<0.01				●		o			
1714	34	0.24					●		o			
1715a	30	0.21					●		o			
1715c	23	0.44	<0.01				●		o			
1767	11	0.73	0.09	0.05 Sb			●			o		
2045	17.5	0.20	0.09				●			o		
2048	20	0.21				●		o	o	o		

CONTINUED ON NEXT PAGE

Table C.1

CONTINUED FROM PREVIOUS PAGE

SAMPLE NUMBER	ALLOY AND IMPURITY ELEMENTS (wt.%)				FRACTURE CLASSIFICATIONS			FRACTURE CLASSIFICATION CODES				
	Ag	Cu	Sn	Pb, Bi, Sb	*PROBABLY* BRITTLE	*POSSIBLY* BRITTLE I	*POSSIBLY* BRITTLE II	*	AAMP	ALDT/C	LDT/C	LDC
2225	25	5.74	0.08				●		○	○		
2313	15	4.89	0.02				●	○	○	○		
2435	21	0.21	0.01				●		○	○		
2437	12	6.87	0.31	trace Sb			●		○	○		
2442	10	8.16	0.27	trace Sb			●			○	○	
3210	5	6.68	0.36	0.04 Pb			●		○	○		
3248	35	0.54	<0.01				●			○		
3445	12	1.72	0.27				●			○		
3446	12	1.21	0.23			●					○	
3448	11	0.88	0.15				●			○		
3449	12	0.96	0.18				●			○		
3461	11	0.41	0.15				●			○		
3608	15	2.39	0.15				●			○		
3610	17.5	3.54	0.20			●		○	○	○		
3611	16	1.80	0.18				●	○	○	○		
3612	15	1.82	0.23				●			○		
3613	15	1.50	0.17				●			○		
3619	20	2.40	0.22			●		○	○		○	
3622	17	2.41	0.09				●		○	○		
3623	17	2.49	0.19			●		○	○			
3624	15	3.50	0.15			●		○	○			
3627	16	2.29	0.11			●		○	○			
3691	18	3.82	0.12				●				○	
3750	23	1.36	0.06			●		○	○	○		
3751	17.5	4.96	0.09				●			○	○	
3753	12.5	4.24	0.18				●			○		
3754	17.5	3.47	0.08				●				○	
3755	17	4.55	0.09			●			○		○	
3756	17.5	4.73	0.23				●			○		
3829	15	0.82	0.07			●		○	○			
3836	10	1.42	0.05				●	○				
3967	14	2.50	0.13	trace Sb		●					○	
4331	22.5	3.05					●			○		

CONTINUED ON NEXT PAGE

Table C.1 CONTINUED FROM PREVIOUS PAGE

SAMPLE NUMBER	ALLOY AND IMPURITY ELEMENTS (wt.%)				FRACTURE CLASSIFICATIONS			FRACTURE CLASSIFICATION CODES				
	Ag	Cu	Sn	Pb, Bi, Sb	*PROBABLY* BRITTLE	*POSSIBLY* BRITTLE I	*POSSIBLY* BRITTLE II	*	AAMP	ALDT/C	LDT/C	LDC
4374	17.5	2.71	0.01	trace Bi		●					○	
4376	35	2.32	0.03	0.03 Pb; 0.02 Bi		●					○	
4434	17.5	0.46					●			○		
4447	7	0.30	<0.01			●		○			○	
4448	30	0.97	<0.01			●		○	○			
4540	10	0.29	0.09				●			○		
4542	12	0.07	0.34				●			○		
4551	9	0.11	<0.01			●		○	○			
4552	12	0.20				●		○	○			
4560	14	3.85	0.17				●			○		
4788	20	3.00	0.07				●		○	○		
4795	16	1.97	0.08				●		○	○		

C.2 Fracture classifications and codes, criteria and examples

The damaged artifacts were assessed from macroscopic photographs and drawings in Hartmann (1970, 1982). This was the only feasible option for the present report. However, as discussed in Appendix C.3, the assessment has enabled suggestions for more definitive investigations.

Table C.1 shows the damaged artifacts consigned to three fracture classifications: *probably* brittle, *possibly* brittle I and *possibly* brittle II, in decreasing order of likelihood. The classifications were made using five fracture classification codes, which are also listed in table C.1.

Table C.2 gives the criteria for the fracture classifications and codes. Nearly all the artifacts are made of thin materials. This greatly complicates the damage assessment, since ductile tears in thin materials can give a macroscopic impression of low ductility or even brittleness.

Figure C.1 quantifies the results of applying the criteria listed in table C.2. Only one artifact, sample number 575, was assessed as *probably* having undergone brittle fracture, Figure C.2 shows this artifact, a highly decorated 20k gold disc, which fulfils all the criteria listed in table C.2, namely:

- many intersecting *and* branching cracks and acute angled missing pieces
- no visible deformation circumjacent to the cracks
- crack, gap and hole edges consisting of rectilinear segments.

Forty-one artifacts were assessed to contain *possibly* brittle I fractures, and ninety-six to contain *possibly* brittle II fractures. Figure C.1 and table C.2 show the distinction between these two classifications is based mainly on whether there were intersecting or branching tears or cracks and any macroscopically visible evidence of circumjacent deformation.

Figures C.3 and C.4 and figures C.5-C.7 respectively give examples of artifacts assessed as containing *possibly* brittle I and *possibly* brittle II fractures. The latter classification is particularly uncertain for thin materials like the ornament and disc in figure C.5, since the damage could well be due to ductile tearing.

Finally, it is important to note that "brittle fracture" does not necessarily mean the material is microstructurally embrittled. It is also possible for brittle-looking damage to be caused by corrosion or stress corrosion cracking, though this seems unlikely for such high-karat artifacts, as discussed in the main text of this report.

C.3 Suggestions for further investigation

Table C.3 shows that more than half the artifacts assessed to contain *probably* brittle (sample 575) or *possibly* brittle I fracture are at two locations, the National Museums of Copenhagen and Dublin. Thus it is reasonable to suggest that more definitive investigations of the nature of the damage to archaeological gold artifacts be done at one or both of these locations.

Firstly one may consider visual inspection and X-ray radiography, in relation to the criteria in table C.2, for a more definitive assessment of the damage. This could be followed, in some cases, by Scanning Electron Microscope (SEM) fractography of whole artifacts (if small, less than about 10 cm in any dimension) or already separate pieces of artifacts. Fractography is a powerful nondestructive diagnostic technique for assessing brittle fracture.

More problematical is metallography. Although it is likely the most important diagnostic technique for assessing damage and embrittlement (Wanhill 1998), metallography is necessarily destructive, however small the specimen taken. On the other hand, in a wider context the eminent metallurgist C.S. Smith demonstrated decades ago how important metallography can be for understanding archaeological metallic artifacts (Smith 1965).

Table C.2 Macroscopically-based criteria for the fracture classifications and codes

*	: intersecting or branching tears or cracks	LDT/C	: low ductility tears or cracks
AAMP	: acute angled missing pieces	LDC	: low ductility cracks
ALDT/C	: *apparently* low ductility tears or cracks		

FRACTURE CLASSIFICATION CODES	FRACTURE CLASSIFICATIONS		
	PROBABLY BRITTLE	*POSSIBLY* BRITTLE I	*POSSIBLY* BRITTLE II
*	• thin *but* • no circumjacent deformation • crack edge rectilinear segments • many cracks ("cracked eggshell" appearance)	• thin *but* • little or no circumjacent deformation • tear or crack edge rectilinear segments	• thin • circumjacent deformation • tear or crack edge curvilinear segments
AAMP	• thin *but* • no circumjacent deformation • gap or hole edge rectilinear segments • many missing pieces	• thin *but* • little or no circumjacent deformation • gap or hole edge rectilinear segments • few missing pieces	• thin • circumjacent deformation • gap or hole edge curvilinear segments • relatively large missing pieces
ALDT/C		• thin • *apparently* little or no circumjacent deformation (visual examination of drawings and photographs only) • tear or crack edge rectilinear segments	• thin • circumjacent deformation • tear or crack edge curvilinear segments
LDT/C		• thin *but* • little or no circumjacent deformation • tear or crack edge rectilinear segments	• thin • little or no circumjacent deformation • indistinctly visible tear or crack edges
LDC		• thin *but* • little or no circumjacent deformation • crack edge rectilinear segments	• thick (very few artifacts) • little or no circumjacent deformation • indistinctly visible or curvilinear crack edges

Table C.3 Sample numbers and museum locations of archaeological gold artifacts illustrated in Hartmann (1970, 1982) and assessed from macroscopic photographs and drawings to contain *probably* brittle (sample 575) or *possibly* brittle I fractures

BML	: British Museum, London	NMA	: National Museum, Athens
DCMD	: Dorset County Museum, Dorchester	NMC	: National Museum, Copenhagen
HMB	: Historical Museum, Bern	NMD	: National Museum, Dublin
NHMV	: Natural History Museum, Vienna		

SAMPLE NUMBER	MUSEUM	SAMPLE NUMBER	MUSEUM	SAMPLE NUMBER	MUSEUM
1	NMD	979	NMD	3619	NMC
341	NHMV	1028	NMD	3623	NMC
346	NHMV	1029	NMD	3624	NMC
450	HMB	1030	NMD	3627	NMC
529	NMD	1045	NMD	3750	NMC
548	NMD	1061	NMD	3755	NMC
555	NMD	1117	NMC	3829	NMC
559	NMD	1491	NHMV	3967	NMC
575	NMD	1492	NHMV	4374	NMA
721	NMD	1493	NHMV	4376	NMA
727	NMD	1494	NHMV	4447	NMA
729	NMD	2048	DCMD	4448	NMA
976	NMD	3446	NMC	4551	BML
977	NMD	3610	NMC	4552	BML

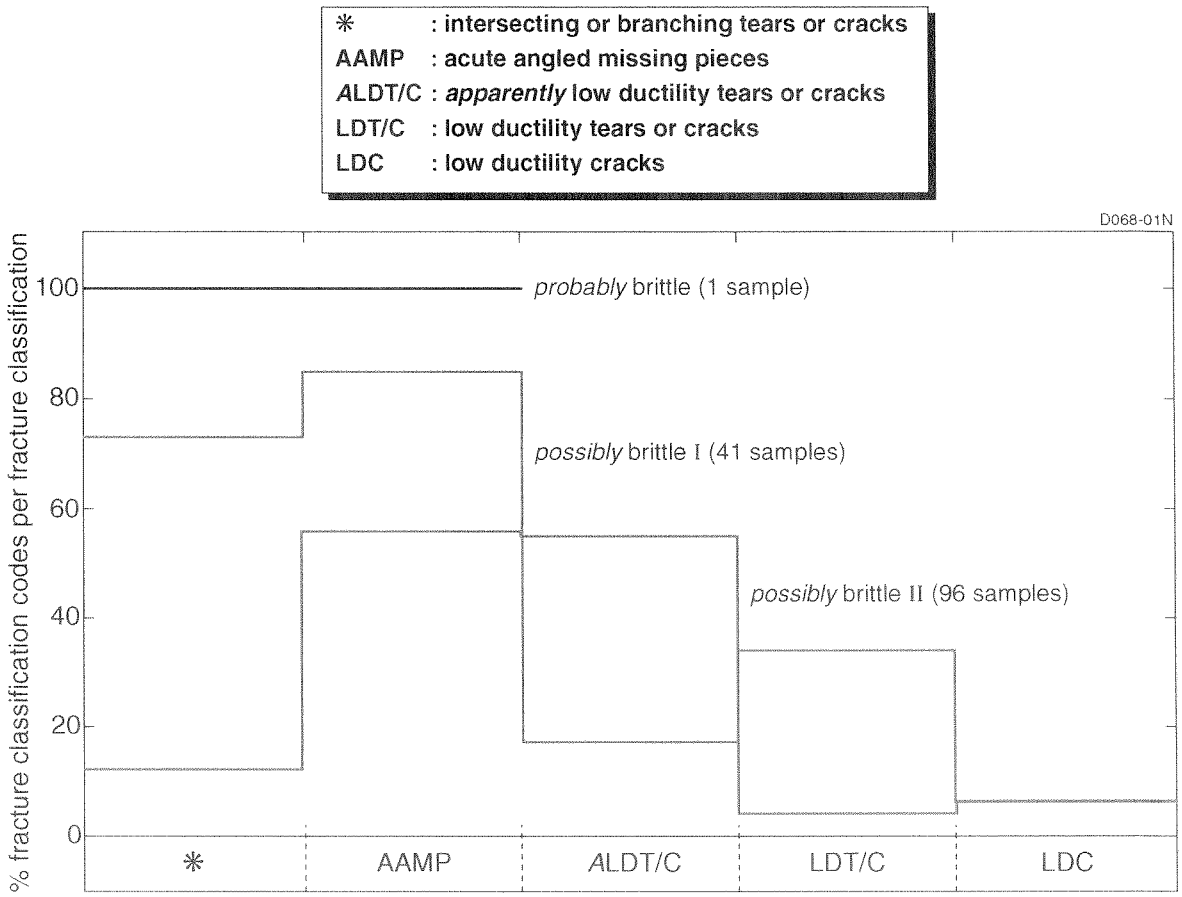

Fig. C.1 Results of applying the criteria listed in table C.2 to damage assessment of the archaeological gold artifacts illustrated in Hartmann (1970, 1982)

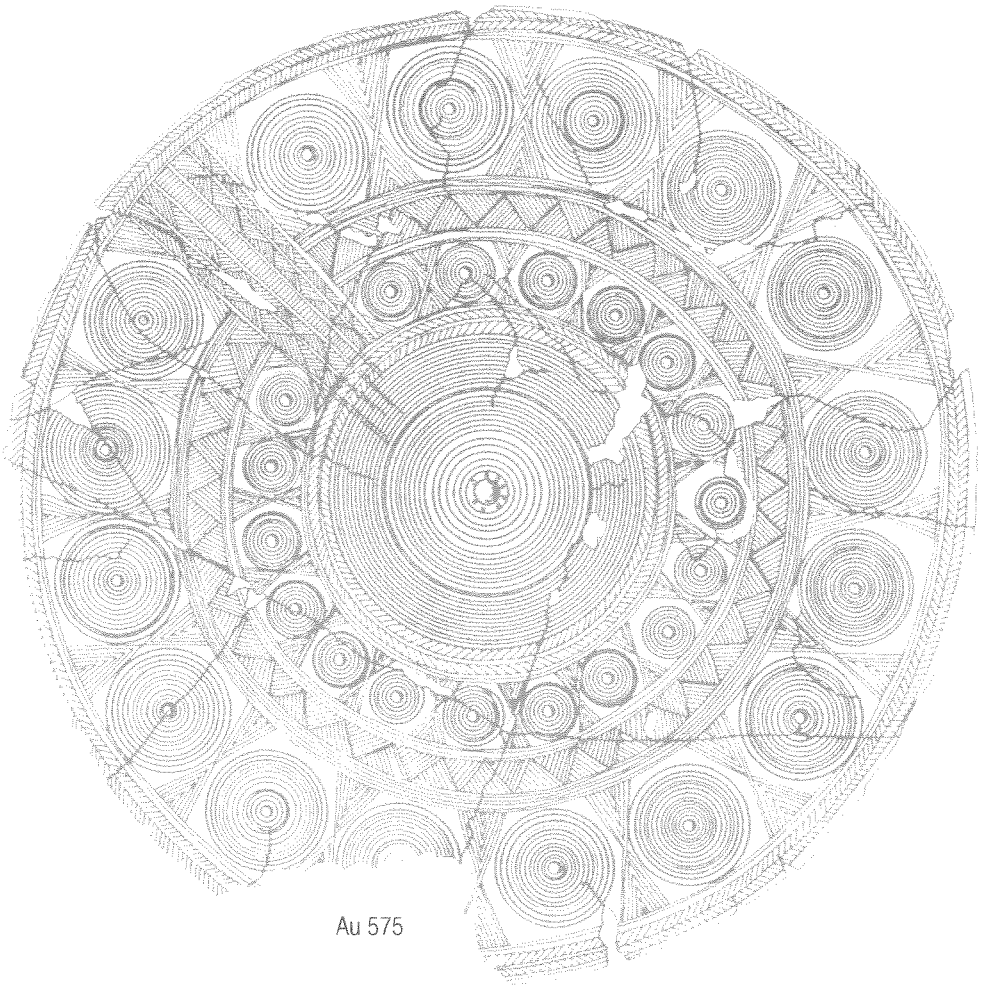

Fig. C.2 Probably *brittle fracture of a 20k archaeological gold disc, composition Au-12 wt. % Ag-4.82 wt. % Cu-0.07 wt. % Sn-0.025 wt. % Pb: National Museum, Dublin. The illustration is from Hartmann (1970), scale 1 : 1, and has been coloured to better indicate the damage*

D068-01N

Fig. C.3 Possibly *brittle I fractures in an 18k archaeological gold collar and a 20k archaeological gold lunula, compositions Au-16 wt. % Ag-7.00 wt. % Cu-0.11 wt. % Sn and Au-1 wt. % Ag-0.09 wt. % Cu-0.06 wt. % Sn, respectively: National Museum, Dublin. The illustrations are from Hartmann (1970), scale 1 : 2, and have been coloured to better indicate the damage*

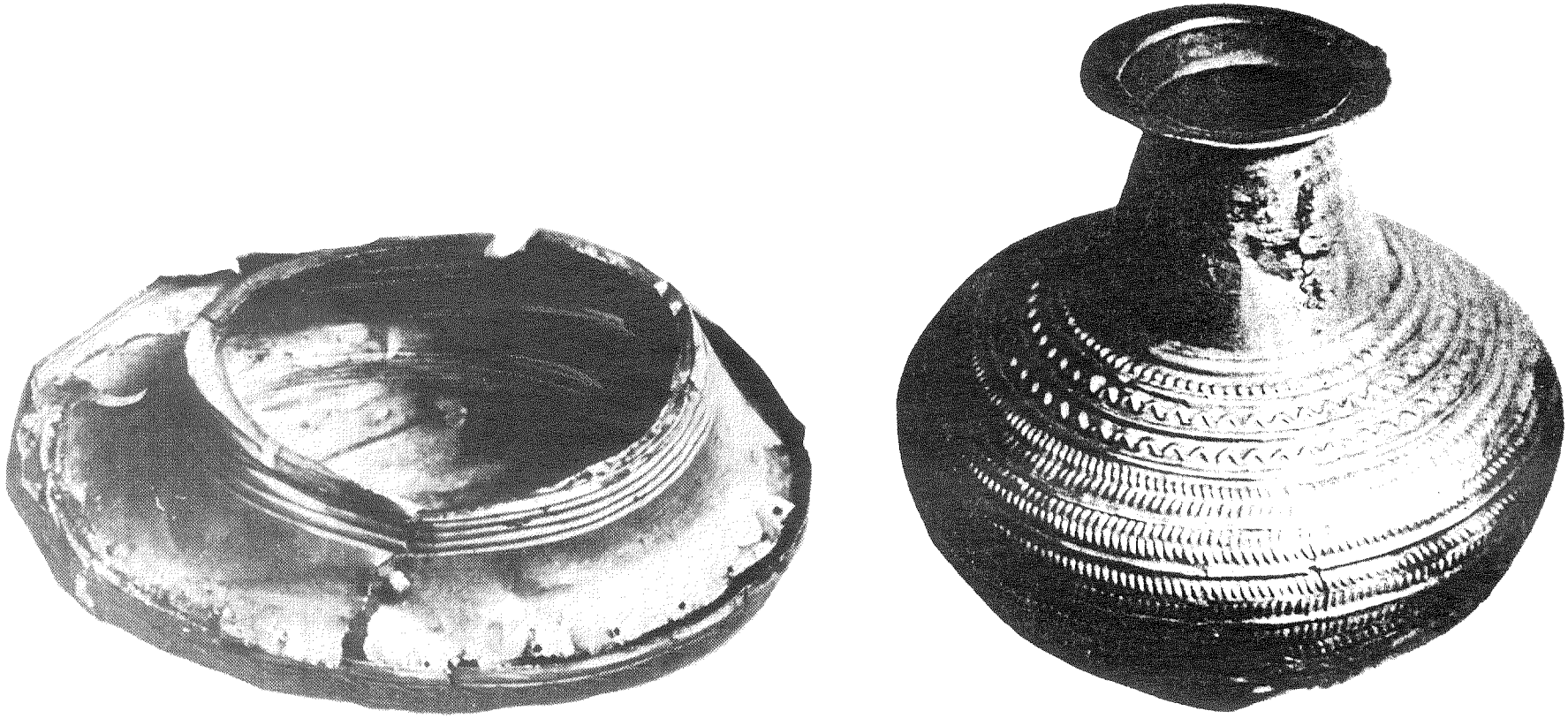

Au 2048

Au 3619

Fig. C.4 Possibly *brittle I fractures in a 19k archaeological gold pommel-cover and an 18.5k archaeological gold vase, compositions Au-20 wt. % Ag-0.21 wt. % Cu and Au-20 wt. % Ag-2.4 wt. % Cu-0.22 wt. % Sn, respectively: the pommel-cover is from the Dorset County Museum, Dorchester, and the vase is from the National Museum, Copenhagen. The photographs are from Hartmann(1982), scale 2 : 1, and 2 : 3 respectively*

Fig. C.5 Possibly brittle II fractures in a 19k archaeological gold collar, ornament and disc, compositions Au-12 wt. % Ag-7.84 wt. % Cu-0.14 wt. % Sn, Au-18 wt. % Ag-2.84 wt. % Cu-0.21 wt. % Sn-trace Bi and Au-15 wt. % Ag-4.89 wt. % Cu-0.02 wt. % Sn, respectively: the collar is from the National Museum, Dublin, the ornament is from the Historical Museum, Bern, and the disc is from the National Museum, Edinburgh. The illustration and photographs are from Hartmann (1970, 1982), scale 1 : 2, 1 : 1 and 1 : 1 respectively, and have been coloured to better indicate the damage

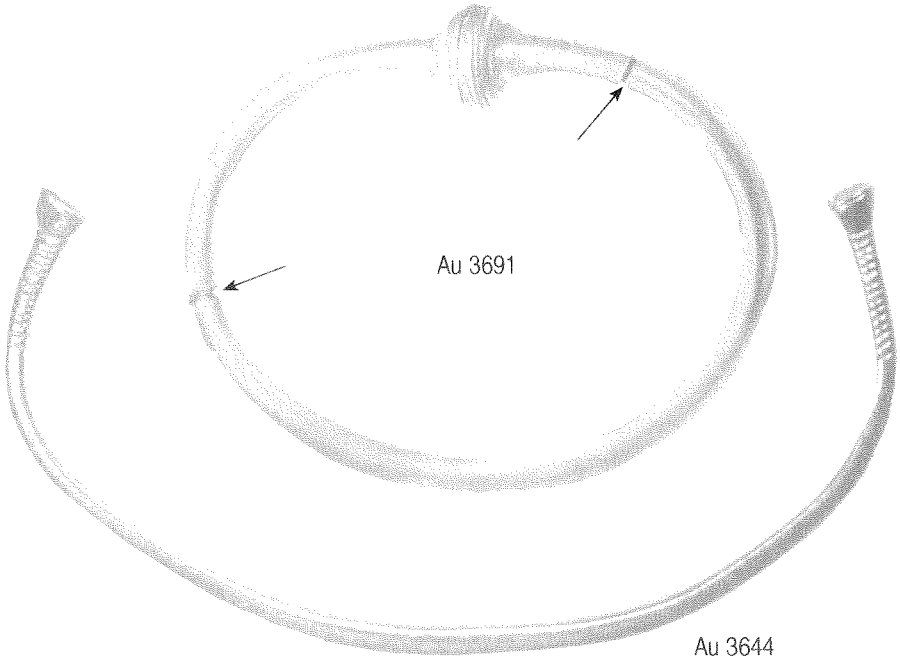

Fig. C.6 Possibly *brittle II fractures (low ductility tears or cracks) in an 18.5k archaeological gold armband compared with ductile deformation of a 19k archaeological gold armband. The compositions are Au-ca. 18 wt. % Ag-4.9 wt. % Cu-0.16 wt. % Sn and Au-16 wt.% Ag-5.1 wt. % Cu-0.18 wt. % Sn, respectively: National Museum, Copenhagen. The photographs are from Hartmann (1982), scale 1 : 1, and have been coloured*

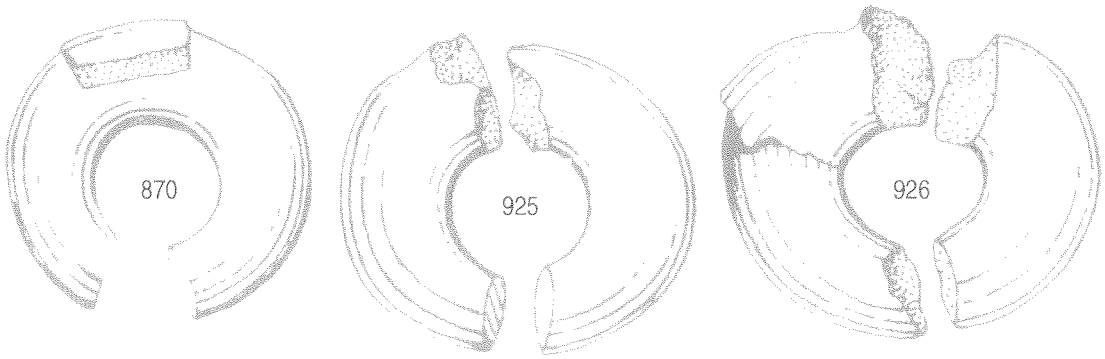

Fig. C.7 Possibly *brittle II fractures (low ductility cracks) in 18.5-20k archaeological gold open rings, compositions Au-17 wt. % Ag-4.82 wt. % Cu-0.38 wt. % Sn, Au-16 wt.% Ag-3.83 wt. % Cu-0.48 wt. % Sn and Au-13 wt. % Ag-3.81 wt. % Cu-0.38 wt. % Sn-trace Pb, respectively: National Museum, Dublin. The illustrations are from Hartmann (1970), scale 2 : 1, and have been coloured*